



# Relations between SMBH Parameters and Jet Generation and Efficiency in Blazars

H. Zhang  and H. J. Zhang

Department of Physics, Yunnan Normal University, Kunming 650092, China; [kmzhanghj@163.com](mailto:kmzhanghj@163.com)  
Received 2023 March 13; revised 2023 July 24; accepted 2023 July 26; published 2023 October 4

## Abstract

We analyzed the relationship between several basic parameters describing supermassive black holes such as jet power, black hole spin, accretion disk magnetic field, black hole mass, etc. We found that there is a general correlation between these parameters, such as jet power is significantly positively correlated with black hole spin, while black hole mass is significantly negatively correlated with black hole spin. To apprehend these relationships, we consider the Blandford–Znajek model to be superior to the Blandford–Payne model. It is also found that the intrinsic gamma luminosity of the FSRQs has a positive correlation with the accretion disk magnetic field, while the intrinsic gamma luminosity of the BL Lacs has a negative correlation with the accretion disk magnetic field. A feedback effect may exist between accretion disk accretion rate and magnetic field, which may be the key to the evolution between BL Lacs and FSRQs. There is no significant difference in the jet power and jet generation efficiency of FSRQs and BL Lacs, which suggests that the jets are generated by the same mechanism. The contribution rate of accretion rate to jet generation efficiency is high, while the contribution rate of accretion rate to jet power is very low.

*Key words:* galaxies: evolution – galaxies: fundamental parameters – galaxies: jets

## 1. Introduction

Active galaxies are a special kind of galaxy that has very violent activities and extreme physical processes, such as generating more energy than what nuclear reaction inside the star provides, generating relativistic high-energy particles and gamma-rays, thus forming non-thermal continuous radiation. Current research believes that these phenomena and processes of active galaxies are mainly produced or triggered by the core of a galaxy. Therefore, the core of an active galaxy is called an active galactic nucleus (AGN). AGNs can be classified as type 1 or type 2 depending on the obscuration of the luminous nucleus. AGNs can also be classified by the angle between the relativistic jet and the line of sight, and the relativistic jets of blazars are believed to be closely aligned to our line of sight. It is found from observations that blazars can be classified into flat-spectrum radio quasars (FSRQs) and BL Lacertae objects (BL Lacs), and while the angle between the jet and the line of sight cannot be used to distinguish them, the accretion rate or accretion model may be the key to their difference. Urry & Padovani (1995) divided blazars into two categories based on the equivalent width (EW) of their emission lines such that objects with  $EW > 5 \text{ \AA}$  are FSRQs, and objects with  $EW < 5 \text{ \AA}$  are BL Lacs (Urry & Padovani 1995). Xiong & Zhang (2014) and Sbarrato et al. (2012) divided blazars by the relation between  $L_\gamma/L_{\text{Edd}}$  and  $L_{\text{BLR}}/L_{\text{Edd}}$  with the dividing line  $L_{\text{BLR}}/L_{\text{Edd}} \sim 5 \times 10^{-4}$ ; FSRQs are greater than the dividing

line while BL Lacs are less than the dividing line, and Ghisellini (2010) divided blazars by the relation between  $\log L_{\text{disk}}/L_{\text{Edd}}$  and  $\log \dot{M}/\dot{M}_{\text{Edd}}$  with the dividing line  $L_{\text{disk}}/L_{\text{Edd}} \sim 10^{-2}$ . The blazars selected in this paper have almost the same dividing line as that of Xiong and Sbarrato. In this paper, an interesting result is obtained, that is, the jet power and accretion disk magnetic field of FSRQs are positively correlated while the jet power and accretion disk magnetic field of BL Lacs are negatively correlated. These results may have important consequences for the evolution of blazars.

The bolometric luminosity is one of the critical parameters controlling the observational properties of AGNs. It can be used to study the sequence of AGNs (Fossati et al. 1997; Ghisellini & Tavecchio 2008; Ghisellini 2010, 2016), the evolution of AGNs (Xie et al. 2004, 2006) and the connection between jet and accretion disk or black hole (Yu et al. 2015; Xue et al. 2016). The bolometric luminosity can be estimated by broad-line region (BLR) luminosity  $L_{\text{bol}} = 10L_{\text{BLR}}$  or by X-ray luminosity  $L_{\text{bol}} = kL_{\text{X}}(2\text{--}10 \text{ keV})$ . The bolometric luminosity is also likely to be related to the beam power, where the beam power of the outflow is defined as the energy per unit time,  $L_j = dE/dt$  (Donato et al. 2001; Giommi et al. 2012; Calderone et al. 2013; Daly et al. 2018; Chen et al. 2021). There are two obvious peaks in the spectral energy distributions (SEDs) of blazars; the low-energy peak is interpreted as caused by synchrotron radiation, and the high energy peak is

interpreted as produced by inverse Compton (IC) scattering. Regarding  $\gamma$ -rays for different energy levels, Mannheim & Biermann (1992) reported that  $\gamma$ -rays of lower-power blazars are produced by the synchrotron-self Compton process and  $\gamma$ -rays of higher-power blazars are produced by the external Compton (EC) process (Sikora et al. 1994). Fossati et al. (1997) calculate the bolometric luminosity by using  $L_\gamma \propto L_{\text{syn,peak}}$ , where  $L_{\text{syn,peak}}$  is the luminosity of the synchrotron radiation peak. In this paper, we use the method of integrating the SED to calculate the bolometric luminosity and compare it with  $L_{\text{bol}} = kL_X(2\text{--}10\text{ keV})$ , finding that the former of BL Lacs is greater than the latter, but we think it has little effect on the correlation analysis.

In regards to black hole systems with powerful jets, the energy of jets may be partly derived from the black hole spin (Blandford & Znajek 1977; Begelman et al. 1984; Meier 1999, 2001; Blandford et al. 2019). Jets may also be related to other parameters, and it is important to understand the relationship between the intrinsic physical variables. Many authors have identified relevant relationships (Rawlings & Saunders 1991; Celotti & Fabian 1993; Maraschi & Tavecchio 2003; Celotti & Ghisellini 2008; Ghisellini et al. 2010; Sbarrato et al. 2012; Ghisellini et al. 2014; Xiong & Zhang 2014; Chen et al. 2015). The intrinsic  $\gamma$ -rays in this paper have a significant correlation with the black hole spin, and we believe that the Blandford–Znajek (1977, hereafter BZ) mechanism may dominate over the Blandford–Payne (1982, hereafter BP) mechanism. In the BZ model, the generation of jets is related to the black hole mass, black hole spin, accretion rate and accretion disk magnetic field, while the BP model is independent of the black hole spin. In a hybrid model (Meier 1999, 2001), because of the existence of a magnetic switch, two distinct slow and fast jets will be produced. For high enough spin, black holes trigger the magnetic switch, and powerful jets will be produced. The lower spin black holes also have jets, but the energy of the jets is dominated by magnetic energy. For the samples in this paper, almost all blazars have sufficiently high spin and highly relativistic jets, but only a few BL Lacs have lower spin. Chen et al. (2021) studied the relationships between the jet powers and accretion rate of rotating supermassive black holes (SMBHs), finding that the contribution of the black hole mass and accretion rate to jet power is more than 95%. The samples in this paper have a similar result.

There may be some unknown relationships between various parameters of blazars. In order to reveal the relationship between them, we have collected 168 data on blazars and the corresponding observation times are in the Space Science Data Center SED Builder (<https://tools.ssd.cas.ac.cn/SED/>) (Stratta et al. 2011). We used these data to calculate the bolometric luminosity, accretion disk magnetic field, etc., and analyze the relationship between them. The methods are introduced in Section 2; the results and discussions are in Section 3; the

summary and conclusions are in Section 4. The cosmological parameters  $H_0 = 69.6\text{ kms}^{-1}\text{ Mpc}^{-1}$ ,  $\Omega_m = 0.286$  and  $\Omega_\Lambda = 0.714$  have been adopted in this work.

## 2. The Methods

### 2.1. The Samples

The black hole masses are from Ghisellini et al. (2014), Xiong & Zhang (2014), Chen et al. (2021). All samples are blazars, and there are 168 blazars in total (including 125 FSRQs and 43 BL Lacs). The virial masses (Shaw et al. 2012) of blazars in our sample have been calculated by assuming the size of the BLR scales, assuming the BLR clouds are bound by the gravity of the central black hole, with the square root of the ionizing disk luminosity as indicated by reverberation mapping, with an average uncertainty of 0.5 dex (Peterson & Wandel 2000; McLure & Dunlop 2004). Nemmen et al. (2012) computed the intrinsic  $\gamma$ -ray luminosity as  $L = f_b L^{\text{iso}}$ , where  $f_b$  is the opening angle or beaming correction factor. For blazar objects,  $f_b$  is computed as  $1 - \cos(1/\Gamma)$ , where  $\Gamma$  is the bulk Lorentz factor. Part of the sources'  $\Gamma$  is from Ghisellini et al. (2014), and part of the sources'  $f_b$  is obtained from Chen et al. (2021). The rest of the sources' intrinsic  $\gamma$ -ray luminosity is obtained from Xiong & Zhang (2014). To get the Lorentz factor we first have to acquire the Doppler factor. For the Doppler factors, the excess frequency of very-long-baseline interferometry (VLBI) can generally be interpreted as being caused by Doppler boosting by comparing the X-rays obtained from VLBI data with those obtained from observations. The Doppler factors can also be obtained using the relationship between the observed brightness temperature and the intrinsic bright temperature, and this method requires significant bursts in the light curve. Once we get the apparent velocity we can calculate the Lorentz factor  $\Gamma = \frac{\beta_{\text{app}}^2 + D^2 + 1}{2D}$  (Hovatta et al. 2009). The accretion disk luminosities are also from Ghisellini et al. (2014), Xiong & Zhang (2014), Chen et al. (2021), with an average uncertainty of 0.3 dex. Nemmen et al. (2012) estimated bolometric luminosity as  $L_{\text{bol}}^{\text{iso}} = L^{\text{iso}} + L_{\text{syn}}^{\text{iso}}$ , but we calculate bolometric luminosity by integrating the SED in this paper. We estimated the power of the jet by using an empirical relation between the average jet power and the radio luminosity, with a scatter of 0.47 dex (Chen et al. 2021). The values of the other parameters will be described below.

### 2.2. Eddington Luminosity

The accretion of massive objects and the associated release of the binding gravitational energy are important sources of radiation in astrophysics. The process depends on the geometry and can be performed via various routes (Netzer 2013). In particular, spherical and nonspherical systems can behave very differently. We assume a black hole with mass  $M$ , monochromatic luminosity  $L_\nu$ , total luminosity  $L$  and fully ionized gas at

a distance  $r$  from the black hole. The radiation pressure force on a particle is

$$f_{\text{rad}} = \frac{N_e \sigma_T}{4\pi r^2 c} \int_0^\infty L_\nu d\nu = \frac{N_e \sigma_T}{4\pi r^2 c} L, \quad (1)$$

where  $N_e$  is the electron density and  $\sigma_T$  is the Thomson cross section. Assuming  $m_\mu$  is the mean mass of particles, the gravitational force per particle is

$$f_g = \frac{GMm_\mu N_e}{r^2}. \quad (2)$$

When  $f_g = f_{\text{rad}}$  the Eddington luminosity,

$$L_{\text{Edd}} = \frac{4\pi c GMm_\mu}{\sigma_T} \simeq a \times 10^{38} (M/M_\odot) \text{erg s}^{-1}, \quad (3)$$

where the Eddington luminosity depends on the value of  $m_\mu$ . According to the definition of the accretion rate  $\dot{M} = L/\epsilon c^2$ , where  $\epsilon$  is the mass-to-luminosity conversion efficiency, the Eddington accretion rate  $\dot{M}_{\text{Edd}} = \frac{L_{\text{Edd}}}{c^2}$ , and the dimensionless accretion rate is  $\dot{m} = \frac{\dot{M}}{\dot{M}_{\text{Edd}}} = \frac{\dot{M}}{L_{\text{Edd}}/c^2} = \frac{\dot{M}c^2}{L_{\text{Edd}}}$ .

### 2.3. Accretion Rate

We can estimate the accretion rate from the part of the SED that shows  $L_\nu \propto \nu^{1/3}$  (Frank et al. 2002; Netzer 2013; Wang et al. 2014). The equation gives the monochromatic luminosity at long wavelengths,

$$L_\nu \simeq 9.4 \times 10^{29} \cos i [M_8 \dot{M}_\odot]^{2/3} \left[ \frac{\lambda}{5100 \text{ \AA}} \right]^{-1/3} \text{erg s}^{-1} \text{Hz}^{-1} \quad (4)$$

where  $M_8$  is the black hole mass in units of  $10^8 M_\odot$ ,  $i$  is the inclination to the line of sight and  $\dot{M}_\odot = \dot{M}/M_\odot \text{yr}^{-1}$ . The mass accretion rate,

$$\dot{M}_\odot \simeq 2.6 \left[ \frac{L_{5100,45}}{\cos i} \right]^{3/2} M_8^{-1}, \quad (5)$$

where  $L_{5100,45}$  is the luminosity at a wavelength of 5100 Å in units of  $10^{45} \text{erg s}^{-1}$ . In the model of the standard disk (Shakura & Sunyaev 1973), Wang et al. (2014) obtained the dimensionless accretion rate using the method above

$$\dot{m} = 20.1 \left( \frac{\ell_{44}}{\cos i} \right)^{3/2} m_7^{-2}, \quad (6)$$

where  $\cos i \approx 0.75$ , which is  $i \approx 40^\circ$ . This estimation result is suitable for Type 1 AGNs with a large angle between the jet and the line of sight, but it is not accurate for blazars.

Ghisellini (2010) reported the relationship between jet power and accretion rate  $P_{\text{jet}} \approx \dot{M}c^2$ , and the relationship between accretion disk luminosity and accretion rate  $L_d \sim 0.1\dot{M}c^2$

$$(\dot{M} \geq \dot{M}_c), \quad L_d \sim 0.1 \left( \frac{\dot{M}}{\dot{M}_c} \right)^2 c^2 \quad (\dot{M} \leq \dot{M}_c), \quad \text{where}$$

$\dot{m}_c = \dot{M}_c/\dot{M}_{\text{Edd}} \sim 10^{-2}-10^{-1}$  (Narayan et al. 1997). Xiong & Zhang (2014) used  $P_{\text{jet}} \approx \dot{M}c^2$  to compute the accretion rate for BL Lacs, and  $L_d \sim 0.1\dot{M}c^2$  to compute the accretion rate for FSRQs, because the jet power is larger than the disk luminosity for BL Lacs while the jet power is smaller than the disk luminosity for FSRQs in his sample. In this paper, the jet power is greater than the accretion disk luminosity for almost all samples, so we use  $P_{\text{jet}} \approx \dot{M}c^2$  to compute accretion rate for all samples, and we also take  $L_d \sim 0.1\dot{M}c^2$  into account. When  $L_d < 10^{-2}L_{\text{Edd}}$  the disk is radiatively inefficient, and depends on advection-dominated accretion flows (ADAFs). The accretion rate will be very low, which is the case for very few BL Lacs in our samples, but they still have powerful jets.

### 2.4. Bolometric Luminosity

All of the methods of estimating the bolometric luminosity are flawed, so we compared the results of the two bolometric luminosity calculations. According to the definition of bolometric luminosity, we can calculate bolometric luminosity by integrating the fitting curve of the SED. The  $\log \nu L_\nu - \log \nu$  figure can be written as

$$\log(\nu L_\nu) = a(\log \nu)^2 + b \log \nu + c. \quad (7)$$

We can replace  $\log \nu$  with  $x$  and  $\log \nu L_\nu$  with  $y$ , then

$$\log L_\nu = y - x = ax^2 + (b-1)x + c, \quad (8)$$

$$L_\nu = 10^{ax^2+(b-1)x+c}, \quad (9)$$

and

$$dx = \frac{d\nu}{\nu \ln 10} \text{ or } 10^x = \nu. \quad (10)$$

Then

$$d\nu = (\nu \ln 10) dx. \quad (11)$$

According to the definition of bolometric luminosity,  $L_{\text{bol}} = \int L_\nu d\nu$

$$dL_{\text{bol}} = L_\nu d\nu = 10^{ax^2+(b-1)x+c} (\nu \ln 10) dx. \quad (12)$$

We can obtain bolometric luminosity

$$L_{\text{bol}} = (\ln 10) * \int_{x_1^{\text{syn}}}^{x_2^{\text{syn}}} 10^{(ax^2+bx+c)} dx + (\ln 10) * \int_{x_1^{\text{IC}}}^{x_2^{\text{IC}}} 10^{(ax^2+bx+c)} dx. \quad (13)$$

Due to the different ranges of synchrotron radiation peaks, the upper and lower limits of the integration should be modified. For low synchrotron peak (LSP) and intermediate synchrotron peak (ISP) objects, the integration range of the synchrotron radiation peak can be set as [7, 17], while for high

synchrotron peak (HSP) cases the integration range of the synchrotron radiation peak can be changed to [7, 21]. The integration range of the IC peak can be uniformly set to [17, 27].

### 2.5. The Spin of Black Holes

The relativistic effects become obvious where the orbits become unstable very close to the black hole. Far from the black hole, where the gravitational field is well approximated by Newton's law of gravity, material follows stable circular orbits. The location of this transition is the innermost stable circular orbit (ISCO). Due to frame dragging effects, the size of the radius of an ISCO is affected by the spin of the black hole, and we can obtain black hole spin by measuring the gravitational redshifts of atomic features in the X-ray spectrum. This is called the X-ray reaction method (Reynolds 2019). The technique is employed most extensively for measuring black hole spin. However, it is very difficult to measure large numbers of samples with this technique, so other methods are considered. Chen et al. (2021) find that the spin of GX 339-4 obtained by the X-ray reaction method is  $0.94 \pm 0.02$ , which is consistent with the result  $0.92 \pm 0.06$  using the method of Daly et al. (2018).

Daly et al. (2018) estimated the black hole spin using the radiation properties of the accretion disk and the properties of the radio source associated with the collimated outflow of the black hole. Daly reported the relationships between bolometric luminosity and beam power for 97 sources,

$$\frac{L_j}{L_{\text{bol}}} \propto \left( \frac{L_{\text{bol}}}{L_{\text{Edd}}} \right)^{\alpha_*} \propto \left( \frac{L_{\text{bol}}}{L_{\text{Edd}}} \right)^{A-1}, \quad (14)$$

where  $\alpha_* = A - 1$ . The fits suggest that  $\alpha_* = -0.5$ . (The exact value is  $\alpha_* = -0.56$ .) The parameterized luminosity of the accretion disk is  $L_{\text{bol}} \propto \dot{\epsilon} M \propto \dot{\epsilon} \dot{m} M$ , and the parameterized beam power is  $L_j \propto \dot{m}^a M^b f(j)$ , where the accretion rate  $\dot{m} \equiv \dot{M}/\dot{M}_{\text{Edd}}$ ,  $f(j)$  is a function of the black hole spin and  $\dot{\epsilon}$  is a dimensionless efficiency factor. Equation (11) with  $\alpha_* = -0.5$  indicates that  $\dot{m}^a M^b f(j) \propto (\dot{\epsilon} \dot{m})^{1/2} M$ , which suggests that  $b = 1$  and  $\dot{m}^a \propto (\dot{\epsilon} \dot{m})^{1/2}$ , and  $L_j/L_{\text{bol}}$  is independent of black hole mass. Considering the simplest solutions  $a = 1$  or  $a = 1/2$ , the first solution indicates  $\dot{\epsilon} \propto \dot{m}$ ,  $L_j \propto \dot{m} M f(j)$  and  $L_{\text{bol}} \propto \dot{m}^2 M$ . The second solution indicates  $\dot{\epsilon} = \text{constant}$ ,  $L_j \propto \dot{m}^{1/2} M f(j)$  and  $L_{\text{bol}} \propto \dot{m} M$ . Compared with existing theoretical models,  $a = 1$  is consistent with the generalized BZ model with a magnetically arrested disk (MAD). Assuming the maximum values of bolometric luminosity and beam power are  $L_{\text{bol}}(\text{max}) = g_{\text{bol}} L_{\text{Edd}}$  and  $L_j(\text{max}) = g_j L_{\text{Edd}}$  respectively, when  $\dot{m} = 1$  and  $\dot{\epsilon} = 1$ , absorbing all constants into the

coefficients yields

$$L_{\text{bol},44} \simeq 130 g_{\text{bol}} (\dot{\epsilon} \dot{m}) M_8, \quad (15)$$

$$L_{j,44} \simeq 130 g_j \dot{m}^a M_8 f(j) / f_{\text{max}}, \quad (16)$$

where  $L_{\text{bol},44}$  and  $L_{j,44}$  are in the unit of  $10^{44} \text{ erg s}^{-1}$ . Combining Equations (12) and (13) with  $\dot{\epsilon} \propto \dot{m}$ , we can obtain

$$\frac{f(j)}{f_{\text{max}}} \simeq \left( \frac{L_{j,44}}{g_j} \right) \left( \frac{130 L_{\text{bol},44} M_8}{g_{\text{bol}}} \right)^{-1/2}. \quad (17)$$

Equation (14) is equal to

$$\frac{f(j)}{f_{\text{max}}} \simeq \left( \frac{L_{j,44}}{g_j} \right) \left( \frac{L_{\text{bol},44}}{g_{\text{bol}}} \right)^{-1/2} (130 M_8)^{-1/2}. \quad (18)$$

Equation (15) is equal to

$$\frac{f(j)}{f_{\text{max}}} \simeq \left( \frac{L_j}{g_j} \right) \left( \frac{L_{\text{bol}}}{g_{\text{bol}}} \right)^{-1/2} (1.3 \times 10^{46} M_8)^{-1/2}, \quad (19)$$

where  $L_{\text{Edd}} = 1.3 \times 10^{38} (M/M_{\odot}) \text{ erg s}^{-1} = 1.3 M_8 \times 10^{46} \text{ erg s}^{-1}$ , then

$$\frac{f(j)}{f_{\text{max}}} = \left( \frac{L_j}{g_j L_{\text{Edd}}} \right) \left( \frac{L_{\text{bol}}}{g_{\text{bol}} L_{\text{Edd}}} \right)^{-A}. \quad (20)$$

In the BZ model (Blandford & Znajek 1977), Tchekhovskoy et al. (2010) and Yuan & Narayan (2014) though numerical simulations suggest that  $\sqrt{f(j)/f_{\text{max}}} = j(1 + \sqrt{1 - j^2})^{-1}$ . We can get the spin of the black hole,  $j$ , in the form

$$j = \frac{2\sqrt{f(j)/f_{\text{max}}}}{f(j)/f_{\text{max}} + 1}. \quad (21)$$

### 2.6. Magnetic Field of Accretion Disk

Modern black hole accretion disk theory suggests that the accretion disk is an MAD, that produces magnetohydrodynamic (MHD) outflows (McKinney et al. 2012). In the BZ model, the Eddington magnetic field is related to black hole mass  $B^2 \propto (\dot{m}/M) \propto M^{-1}$  (Rees 1984; Blandford et al. 2019). Daly (2019) thinks the Eddington magnetic field has a pressure similar to that of a radiation field with the Eddington luminosity, thus, the form of the beam power,

$$\frac{L_j}{L_{\text{Edd}}} = g_j \left( \frac{B}{B_{\text{Edd}}} \right)^2 \left( \frac{f(j)}{f_{\text{max}}} \right). \quad (22)$$

Combining Equations (17) and (19)

$$\left( \frac{B}{B_{\text{Edd}}} \right)^2 = \left( \frac{L_{\text{bol}}}{g_{\text{bol}} L_{\text{Edd}}} \right)^A. \quad (23)$$

**Table 1**  
The Samples

Name [1]	$z$ [2]	Type [3]	$\log M$ [4]	$\log B$ [5]	$\log P_{\text{jet}}$ [6]	$\log j$ [7]	$\log L_{\text{disk}}$ [8]	$\log \eta_m$ [9]	$\log L_{\gamma}^{\text{int}}$ [10]	$\log f_b$ [11]
2FGL J1203.2+6030	0.065	BZB	8.6	4.12	44.33	-1.48	43.00	-4.72	42.57	-2.65
2FGL J1221.4+2814	0.103	BZB	8.6	4.33	45.05	-1.37	43.08	-4.50	43.04	-2.30
2FGL J1420.2+5422	0.153	BZB	8.3	4.54	45.39	-1.04	43.26	-3.84	42.74	-2.30
2FGL J0831.9+0429	0.174	BZB	8.5	4.46	45.51	-1.08	43.65	-3.92	43.42	-2.30
2FGL J0013.8+1907	0.477	BZB	8.3	4.68	45.28	-1.33	43.78	-4.42	43.77	-2.38
1FGL J0430.4-2509	0.516	BZB	6.51	5.96	45.17	-0.69	43.95	-3.12	43.82	-2.38
1FGL J1043.1+2404	0.559	BZB	8.09	4.89	45.44	-0.86	44.68	-3.48	44.21	-2.21
2FGL J1540.4+1438	0.606	BZB	8.5	4.61	46.06	-0.42	44.56	-2.53	44.15	-2.30
1FGL J0217.0-0829	0.607	BZB	6.53	5.98	45.68	-0.23	44.20	-2.08	43.84	-2.53
2FGL J1824.0+5650	0.664	BZB	8.5	4.69	45.78	-0.51	44.91	-2.74	44.54	-2.30
1FGL J2236.2+2828	0.790	BZB	8.35	4.86	45.53	-0.89	45.38	-3.53	44.86	-2.38
1FGL J2315.9-5014	0.808	BZB	7.68	5.26	45.80	-0.68	44.65	-3.09	44.21	-2.53
2FGL J2152.4+1735	0.874	BZB	8.8	4.45	46.18	-0.68	45.18	-3.10	44.56	-2.30
2FGL J2247.2-0002	0.949	BZB	8.8	4.49	45.64	-0.84	45.13	-3.43	44.64	-2.38
1FGL J1734.4+3859	0.975	BZB	7.97	5.20	45.43	-0.80	45.30	-3.35	45.10	-2.53
1FGL J0725.3+1431	1.038	BZB	8.31	4.95	45.98	-0.61	45.95	-2.95	45.06	-2.59
2FGL J2206.6-0029	1.053	BZB	8.5	4.71	46.39	-1.00	44.83	-3.75	44.65	-2.38
1FGL J1037.7-2820	1.066	BZB	8.99	4.37	46.53	-0.90	46.03	-3.56	44.65	-2.46
1FGL J0407.5+0749	1.133	BZB	8.65	4.64	46.64	-0.69	45.78	-3.12	44.76	-2.46
2FGL J2244.1+4059	1.171	BZB	8.28	4.95	46.15	-0.73	45.38	-3.20	44.85	-2.59
1FGL J2031.5+1219	1.213	BZB	7.59	5.43	46.25	-0.29	44.88	-2.21	44.57	-2.81
2FGL J0334.2-4008	1.357	BZB	8.6	4.81	46.73	-0.75	44.86	-3.24	45.01	-2.76
1FGL J0058.0+3314	1.369	BZB	7.99	5.12	46.27	-0.91	45.18	-3.57	44.84	-2.53
1FGL J1123.9+2339	1.549	BZB	8.79	4.57	46.26	-0.67	45.83	-3.08	44.86	-2.53
1FGL J1133.1+0033	1.633	BZB	8.8	4.71	46.26	-0.67	45.88	-3.07	45.50	-2.59
2FGL J0629.3-2001	1.724	BZB	8.5	4.89	46.34	-0.64	45.13	-3.00	45.53	-2.38
2FGL J1310.6+3222	0.996	BZB	8.48	4.84	46.70	-0.58	45.92	-2.88	44.58	-2.38
2FGL J1727.1+4531	0.717	BZB	8.22	4.87	46.57	-0.72		-3.17	44.40	-2.49
2FGL J0608.0-0836	0.870	BZB	7.63	5.37	46.39	-0.21	45.60	-2.01	44.69	-3.01
4FGL J0449.1+1121	2.153	BZB	7.89	5.47	46.73	-0.32	45.92	-2.29	45.97	-2.53
1FGL J1058.4+0134	0.888	BZB	7.37	5.62	46.23	-0.13	45.51	-1.75	44.88	-2.59
2FGL J0238.7+1637	0.940	BZB	9	4.53	46.98	-0.87	44.92	-3.50	44.72	-2.66
2FGL J0721.9+7120	0.300	BZB	8.1	5.00	46.16	-0.81		-3.36	44.46	-2.32
2FGL J0738.0+1742	0.424	BZB	8.4	4.74	46.87	-0.69		-3.11	44.19	-2.38
2FGL J0757.1+0957	0.266	BZB	8.2	4.73	46.52	-0.89		-3.52	42.75	-2.97
2FGL J0825.9+0308	0.506	BZB	8.83	4.36	46.37	-0.88	44.37	-3.52	43.73	-2.14
2FGL J0854.8+2005	0.306	BZB	8.8	4.41	47.03	-1.14	44.58	-4.03	43.89	-2.23
2FGL J1015.1+4925	0.212	BZB	8.3	4.78	46.49	-1.17		-4.11	43.83	-2.11
2FGL J1217.8+3006	0.130	BZB	8.12	4.80	46.47	-1.10		-3.96	43.28	-1.90
2FGL J1751.5+0938	0.322	BZB	8.7	4.45	46.48	-0.62	44.70	-2.97	44.16	-2.10
2FGL J1800.5+7829	0.680	BZB	8.6	4.68	46.73	-0.66	45.85	-3.04	44.83	-2.25
2FGL J1806.7+6948	0.051	BZB	8.7	4.09	46.17	-0.97	43.00	-3.69	44.08	-0.34
2FGL J2202.8+4216	0.069	BZB	8.23	4.58	46.93	-1.17	43.52	-4.11	43.40	-1.77
1FGL J0017.4-0510	0.226	BZQ	7.55	5.09	46.36	-0.86	44.65	-3.48	43.14	-2.46
1FGL J0422.0-0647	0.242	BZQ	7.47	5.13	46.91	-1.01	44.49	-3.78	43.06	-2.46
1FGL J0937.7+5005	0.276	BZQ	7.5	5.14	46.30	-1.12	43.78	-4.01	43.15	-2.38
1FGL J1505.0+0328	0.409	BZQ	7.41	5.30	46.80	-0.85	44.83	-3.45	43.62	-2.59
1FGL J2117.8+0016	0.463	BZQ	7.745	4.97	46.65	-0.73	44.78	-3.20	43.12	-2.46
1FGL J0714.0+1935	0.540	BZQ	7.62	5.28	46.75	-0.75	44.78	-3.24	44.35	-2.46
1FGL J2331.0-2145	0.563	BZQ	7.58	5.25	46.40	-0.97	44.88	-3.69	44.09	-2.46
1FGL J1514.7+4447	0.570	BZQ	7.67	5.16	46.83	-0.94	44.30	-3.63	43.99	-2.38
1FGL J0949.0+0021	0.585	BZQ	7.595	5.34	46.90	-1.02	45.35	-3.80	44.20	-2.65
1FGL J2035.4+1100	0.601	BZQ	8	5.06	46.56	-0.65	45.18	-3.03	44.43	-2.46
1FGL J1023.6+3937	0.604	BZQ	8.95	4.26	46.68	-0.60	45.88	-2.92	43.95	-2.38
1FGL J0509.2+1015	0.621	BZQ	8.275	4.78	47.07	-0.72	45.26	-3.19	44.18	-2.46
1FGL J0721.4+0401	0.665	BZQ	8.805	4.41	47.19	-1.21	46.26	-4.18	44.06	-2.53
1FGL J1954.8-1124	0.683	BZQ	6.73	5.94	46.81	-0.36	44.48	-2.39	44.56	-2.38
1FGL J1351.0+3035	0.712	BZQ	8.27	4.78	46.49	-0.88	45.54	-3.50	44.09	-2.46

**Table 1**  
(Continued)

Name [1]	$z$ [2]	Type [3]	$\log M$ [4]	$\log B$ [5]	$\log P_{\text{jet}}$ [6]	$\log j$ [7]	$\log L_{\text{disk}}$ [8]	$\log \eta_m$ [9]	$\log L_{\gamma}^{\text{int}}$ [10]	$\log f_b$ [11]
IFGL J1830.1+0618	0.745	BZQ	8.775	4.50	47.09	-0.87	46.35	-3.50	44.49	-2.53
IFGL J1848.5+3224	0.800	BZQ	8.04	5.04	47.17	-0.72	45.65	-3.19	44.43	-2.53
IFGL J0540.9-0547	0.838	BZQ	8.74	4.53	46.68	-0.62	46.02	-2.97	44.48	-2.53
IFGL J1106.5+2809	0.843	BZQ	8.85	4.42	47.12	-1.32	45.20	-4.40	44.45	-2.38
IFGL J0442.7-0019	0.845	BZQ	8.1	5.11	46.45	-0.52	45.78	-2.76	45.08	-2.53
IFGL J0456.4-3132	0.865	BZQ	8.195	4.87	46.09	-0.96	45.48	-3.67	44.22	-2.53
IFGL J0004.7-4737	0.880	BZQ	7.85	5.15	46.50	-0.53	45.32	-2.76	44.26	-2.59
IFGL J2025.9-2852	0.884	BZQ	8.34	4.79	47.04	-0.90	45.05	-3.55	44.43	-2.53
IFGL J0957.7+5523	0.888	BZQ	8.45	4.87	46.63	-0.42	45.65	-2.52	45.36	-2.38
IFGL J1443.8+2457	0.939	BZQ	7.63	5.31	47.48	-0.48	45.26	-2.65	44.71	-2.30
IFGL J1321.1+2214	0.943	BZQ	8.315	4.92	47.01	-0.97	45.38	-3.70	44.78	-2.53
IFGL J1359.1+5539	1.014	BZQ	8	5.04	47.10	-0.86	45.13	-3.48	44.38	-2.53
IFGL J0909.0+0126	1.026	BZQ	9.14	4.34	47.42	-0.84	46.53	-3.42	44.83	-2.53
IFGL J1709.6+4320	1.027	BZQ	7.92	5.16	47.18	-0.75	45.18	-3.24	44.64	-2.65
IFGL J1033.8+6048	1.064	BZQ	8.75	4.61	46.95	-0.68	45.38	-3.09	44.82	-2.59
IFGL J1146.8+4004	1.088	BZQ	8.93	4.48	46.82	-0.93	46.07	-3.61	44.89	-2.46
IFGL J0608.0-1521	1.094	BZQ	8.09	5.08	46.97	-0.70	45.56	-3.14	44.86	-2.59
IFGL J1033.2+4116	1.117	BZQ	8.61	4.68	46.86	-0.56	45.78	-2.84	44.60	-2.59
IFGL J2212.1+2358	1.125	BZQ	8.46	4.83	46.62	-0.91	45.78	-3.58	44.94	-2.53
IFGL J1609.0+1031	1.232	BZQ	8.77	4.67	46.56	-0.75	46.26	-3.25	45.22	-2.46
IFGL J0438.8-1250	1.285	BZQ	8.66	4.63	47.11	-0.68	45.80	-3.09	44.86	-2.38
IFGL J1347.8-3751	1.300	BZQ	8.285	4.99	46.98	-0.84	45.73	-3.42	45.19	-2.46
IFGL J1553.4+1255	1.308	BZQ	8.64	4.75	46.55	-0.55	46.78	-2.82	45.30	-2.46
IFGL J1802.5-3939	1.319	BZQ	8.595	5.03	47.10	-0.63	46.18	-2.99	46.46	-2.46
IFGL J1209.3+5444	1.344	BZQ	8.4	4.86	46.88	-0.83	45.62	-3.41	44.84	-2.59
IFGL J2145.4-3358	1.361	BZQ	8.31	4.92	47.04	-1.00	45.35	-3.75	44.94	-2.53
IFGL J1333.2+5056	1.362	BZQ	7.95	5.19	47.04	-0.82	45.38	-3.38	44.84	-2.65
IFGL J0245.9-4652	1.385	BZQ	8.4	4.95	47.17	-0.37	46.38	-2.40	45.35	-2.46
IFGL J0257.8-1204	1.391	BZQ	9.22	4.23	46.97	-1.10	46.35	-3.97	44.85	-2.38
IFGL J1613.5+3411	1.400	BZQ	9.08	4.45	47.33	-0.61	46.73	-2.94	45.30	-2.30
IFGL J1033.8+6048	1.401	BZQ	9.09	4.43	46.82	-0.72	45.71	-3.17	45.05	-2.65
IFGL J1326.6+2213	1.403	BZQ	9.25	4.35	47.23	-1.00	46.02	-3.75	45.24	-2.53
IFGL J1550.7+0527	1.417	BZQ	8.98	4.48	46.82	-0.50	46.08	-2.70	45.05	-2.46
IFGL J0825.0+5555	1.418	BZQ	9.1	4.37	47.32	-0.50	46.35	-2.72	44.78	-2.59
IFGL J0252.8-2219	1.419	BZQ	9.4	4.23	46.92	-0.81	45.50	-3.36	45.46	-2.46
IFGL J1804.1+0336	1.420	BZQ	7.79	5.27	47.26	-0.24	45.08	-2.08	44.66	-2.65
IFGL J2157.4+3129	1.448	BZQ	8.89	4.57	47.06	-0.69	45.73	-3.12	45.20	-2.53
IFGL J2322.0+3208	1.489	BZQ	8.705	4.67	47.50	-0.66	45.73	-3.06	45.14	-2.46
IFGL J1332.6-1255	1.492	BZQ	8.785	4.64	46.97	-0.93	46.26	-3.61	45.18	-2.65
IFGL J0011.1+0050	1.493	BZQ	8.445	4.82	47.20	-0.92	45.56	-3.60	44.91	-2.53
IFGL J1436.9+2314	1.548	BZQ	8.31	4.93	47.09	-0.52	46.17	-2.76	45.07	-2.38
IFGL J2110.0+0811	1.580	BZQ	8.82	4.58	47.47	-1.15	46.05	-4.06	45.11	-2.53
IFGL J1358.1+7646	1.585	BZQ	8.255	4.97	47.11	-0.66	45.18	-3.05	44.84	-2.65
IFGL J1016.1+0514	1.714	BZQ	7.99	5.26	47.15	-0.51	45.65	-2.73	45.59	-2.46
IFGL J1228.2+4855	1.722	BZQ	8.255	4.99	47.05	-0.32	45.65	-2.29	45.13	-2.46
IFGL J0254.2+5107	1.732	BZQ	8.74	4.75	47.00	-0.73	46.02	-3.19	45.61	-2.59
IFGL J2327.7+0943	1.841	BZQ	9.025	4.59	47.47	-0.85	46.48	-3.45	45.56	-2.46
IFGL J1112.8+3444	1.956	BZQ	8.78	4.67	47.75	-0.81	46.28	-3.36	45.54	-2.30
2FGL J0438.8-4521	2.017	BZQ	8.5	4.87	47.25	-0.91	45.26	-3.58	45.36	-2.38
IFGL J0023.0+4453	2.023	BZQ	7.78	5.36	47.69	-0.49	45.43	-2.68	45.07	-2.65
IFGL J0325.9+2219	2.066	BZQ	9.33	4.35	47.25	-0.86	46.78	-3.46	45.59	-2.46
IFGL J1959.3-4241	2.178	BZQ	8.98	4.58	45.90	-1.11	46.16	-3.98	45.57	-2.46
IFGL J2120.9+1901	2.180	BZQ	7.75	5.44	46.97	-0.26	45.78	-2.13	45.58	-2.53
IFGL J2135.8-4957	2.181	BZQ	8.355	4.97	46.79	-0.60	46.12	-2.93	45.15	-2.71
IFGL J0920.9+4441	2.189	BZQ	9.29	4.49	47.83	-0.74	46.71	-3.23	46.23	-2.46
IFGL J1539.7+2747	2.191	BZQ	8.47	4.88	46.95	-0.79	45.65	-3.33	45.33	-2.46
IFGL J0245.4+2413	2.243	BZQ	9.1	4.47	47.21	-0.64	46.32	-3.01	45.38	-2.59
IFGL J0157.5-4613	2.287	BZQ	8.25	5.04	47.25	-0.63	45.78	-2.99	45.22	-2.59

**Table 1**  
(Continued)

Name [1]	$z$ [2]	Type [3]	$\log M$ [4]	$\log B$ [5]	$\log P_{\text{jet}}$ [6]	$\log j$ [7]	$\log L_{\text{disk}}$ [8]	$\log \eta_m$ [9]	$\log L_{\gamma}^{\text{int}}$ [10]	$\log f_b$ [11]
1FGL J1152.2-0836	2.367	BZQ	9.38	4.30	47.05	-0.85	46.28	-3.46	45.56	-2.53
1FGL J1344.2-1723	2.506	BZQ	9.12	4.55	46.86	-0.93	46.03	-3.61	45.70	-2.76
1FGL J1345.4+4453	2.534	BZQ	8.98	4.60	46.89	-0.78	46.02	-3.31	45.68	-2.59
1FGL J0912.3+4127	2.563	BZQ	9.32	4.29	46.57	-0.62	46.35	-2.96	45.54	-2.38
1FGL J0911.0+2247	2.661	BZQ	8.7	4.77	47.08	-0.82	46.18	-3.39	45.40	-2.71
1FGL J0746.6+2548	2.979	BZQ	9.23	4.52	47.09	-0.91	46.48	-3.57	45.57	-2.71
2FGL J0108.6+0135	2.107	BZQ	8.83	4.77	47.18	-0.31	47.13	-2.28	45.43	-3.21
1FGL J0237.9+2848	1.206	BZQ	9.22	4.38	47.11	-0.69	46.26	-3.11	45.27	-2.53
2FGL J0530.8+1333	2.060	BZQ	9.8	4.15	46.89	-1.04		-3.84	45.36	-2.96
4FGL J0532.6+0732	1.254	BZQ	8.43	4.90	46.28	-0.45	45.86	-2.59	44.98	-2.59
2FGL J0739.2+0138	0.189	BZQ	8.11	4.73	47.44	-0.71	45.19	-3.16	42.91	-2.74
2FGL J0750.6+1230	0.889	BZQ	8.15	5.00	47.19	-0.44	45.95	-2.57	44.47	-2.52
2FGL J0830.5+2407	0.940	BZQ	8.95	4.46	47.49	-0.83	45.97	-3.41	44.07	-3.10
2FGL J0841.6+7052	2.172	BZQ	9.36	4.49	47.63	-0.54	47.43	-2.80	45.16	-3.20
2FGL J0909.1+0121	1.024	BZQ	9	4.44	46.54	-0.73	46.24	-3.20	44.86	-2.74
2FGL J0921.9+6216	1.453	BZQ	8.93	4.49	47.10	-0.56	46.05	-2.83	44.71	-2.67
2FGL J0948.8+4040	1.249	BZQ	8.95	4.44	46.57	-0.40	46.50	-2.49	43.71	-3.28
2FGL J0957.7+5522	0.896	BZQ	8.34	4.95	47.31	-0.35	45.57	-2.36	44.93	-2.77
2FGL J1159.5+2914	0.724	BZQ	8.5	4.81	46.90	-0.52	45.71	-2.76	44.21	-3.10
2FGL J1222.4+0413	0.965	BZQ	8.31	4.96	47.41	-0.46	45.86	-2.61	44.70	-2.65
2FGL J1258.2+3231	0.806	BZQ	8.5	4.67	47.57	-0.78	45.54	-3.31	44.15	-2.31
2FGL J1326.8+2210	1.400	BZQ	9.25	4.35	46.48	-0.90	45.96	-3.56	44.92	-2.77
2FGL J1419.4+3820	1.831	BZQ	8.62	4.79	47.20	-0.60	46.10	-2.93	44.85	-2.73
2FGL J1436.9+2319	1.548	BZQ	8.38	4.88	46.88	-0.51	45.78	-2.73	44.54	-2.56
2FGL J1522.1+3144	1.484	BZQ	8.92	4.70	47.04	-0.88	45.90	-3.50	45.42	-3.13
2FGL J1549.5+0237	0.414	BZQ	8.62	4.49	46.95	-0.83	45.83	-3.40	43.98	-2.27
2FGL J1550.7+0526	1.422	BZQ	9.18	4.34	46.72	-0.49	46.08	-2.68	44.69	-2.64
2FGL J1608.5+1029	1.226	BZQ	8.97	4.58	47.49	-0.56	46.01	-2.84	44.70	-2.85
2FGL J1613.4+3409	1.397	BZQ	9.34	4.26	46.14	-0.61	46.46	-2.95	44.88	-2.11
2FGL J1635.2+3810	1.814	BZQ	9.37	4.43	47.70	-0.68	46.67	-3.09	45.44	-3.29
2FGL J1740.2+5212	1.375	BZQ	9.32	4.33	47.48	-0.83	46.16	-3.40	45.01	-2.81
2FGL J1849.4+6706	0.657	BZQ	9.14	4.34	47.25	-0.97	45.42	-3.70	44.63	-2.61
2FGL J2148.2+0659	0.990	BZQ	8.87	4.55	46.56	-0.53	46.77	-2.78	44.77	-2.10
2FGL J2211.9+2355	1.125	BZQ	8.46	4.83	46.60	-0.73	45.79	-3.21	44.39	-2.47
2FGL J2232.4+1143	1.037	BZQ	8.78	4.69	47.20	-0.47	46.87	-2.64	44.89	-2.68
2FGL J2253.9+1609	0.859	BZQ	8.83	4.82	47.25	-0.56	46.65	-2.84	45.91	-2.88
2FGL J0102.7+5827	0.644	BZQ	7.57	5.38	46.98	-0.51	45.66	-2.74	44.55	-2.38
2FGL J0245.1+2406	2.247	BZQ	9.08	4.49	46.94	-0.59	46.34	-2.91	45.39	-2.94
2FGL J0533.0+4823	1.160	BZQ	9.25	4.33	46.10	-0.88	46.26	-3.52	45.17	-2.53
2FGL J0840.7+1310	0.680	BZQ	7.62	5.24	46.39	-0.04	45.75	-1.39	44.09	-2.46
2FGL J1317.9+3426	1.055	BZQ	9.14	4.24	45.93	-0.61	46.07	-2.95	44.50	-2.38
2FGL J1504.3+1029	1.839	BZQ	7.98	5.44	46.42	-0.50	46.30	-2.70	46.07	-2.81
2FGL J2334.3+0734	0.401	BZQ	7.37	5.34	46.20	-0.59	45.93	-2.89	43.64	-2.46
1FGL J0806.2+6148	3.033	BZQ	9.07	4.58	46.30	-0.61	46.52	-2.95	45.61	-2.65
4FGL J0532.6+0732	1.254	BZQ	8.43	4.91	46.53	-0.45	45.86	-2.59	45.20	-2.59
1FGL J0654.3+4514	0.928	BZQ	8.17	5.00	45.27	-0.64	45.25	-3.00	44.94	-2.46
1FGL J0956.9+2513	0.707	BZQ	8.88	4.39	45.15	-0.83	45.93	-3.41	44.38	-2.30
1FGL J2229.7-0832	1.560	BZQ	8.62	4.88	46.48	-0.44	46.45	-2.58	45.60	-2.53
2FGL J0136.9+4751	0.859	BZQ	8.3	4.96	46.22	-0.59	45.44	-2.91	44.95	-2.62
2FGL J0924.0+2819	0.744	BZQ	8.8	4.43	46.75	-0.76	45.63	-3.26	44.20	-2.34
2FGL J1014.1+2306	0.566	BZQ	8.54	4.56	45.02	-0.49	45.89	-2.68	43.86	-2.21
2FGL J1224.9+2122	0.432	BZQ	8.87	4.48	45.28	-0.70	46.21	-3.15	43.90	-3.61

**Note.** The first column is the name of Fermi blazars; the second column is the redshift; the third column is the class of Fermi blazars; the fourth column is the logarithm of the black hole mass; the fifth column is the logarithm of the accretion disk magnetic field; the sixth column is the logarithm of the jet power; the seventh column is the logarithm of the black hole spin; the eighth column is the logarithm of the disk luminosity; the ninth column is the jet generation efficiency; the tenth column is the logarithm of the intrinsic  $\gamma$ -ray luminosity; the eleventh column is the logarithm of the beaming factor.

**Table 2**  
 The Samples

Dependent Variable [1]	Independent Variable [2]	Class [3]	Slope [4]	Intercept [5]	$P$ [6]	Correlation Strength [7]
$\log M$	$\log B$	FSRQs	-1.57	16.03	$5.21 \times 10^{-59}$	strong
$\log M$	$\log B$	BL Lacs	-1.16	13.89	$2.48 \times 10^{-17}$	strong
$\log j$	$\log M$	FSRQs	-0.075	-0.062	$3 \times 10^{-2}$	strong
$\log j$	$\log M$	BL Lacs	-0.24	-1.22	$4 \times 10^{-2}$	strong
$\log \dot{M}_{\text{jet}}$	$\log j$	FSRQs	0.995	30.56	$1.55 \times 10^{-6}$	strong
$\log \dot{M}_{\text{jet}}$	$\log j$	BL Lacs	1.77	30.76	$6.4 \times 10^{-9}$	strong
$\log L_{\gamma}^{\text{int}}$	$\log L_{\text{disk}}$	FSRQs	0.6436	15.32	$2.55 \times 10^{-12}$	strong
$\log L_{\gamma}^{\text{int}}$	$\log L_{\text{disk}}$	BL Lacs	0.7098	12.58	$8.61 \times 10^{-12}$	strong
$\log L_{\gamma}^{\text{int}}$	$\log M$	FSRQs	0.5582	40.05	$1.36 \times 10^{-8}$	strong
$\log L_{\gamma}^{\text{int}}$	$\log M$	BL Lacs	0.0745	43.7	0.73	week
$\log L_{\gamma}^{\text{int}}$	$\log j$	FSRQs	0.3829	45.09	0.16	week
$\log L_{\gamma}^{\text{int}}$	$\log j$	BL Lacs	1.475	45.47	$2.65 \times 10^{-5}$	strong
$\log P_{\text{jet}}$	$\log j$	FSRQs	0.9954	47.51	$1.55 \times 10^{-6}$	strong
$\log P_{\text{jet}}$	$\log j$	BL Lacs	1.7666	47.72	$6.4 \times 10^{-9}$	strong
$\log P_{\text{jet}}$	$\log M$	FSRQs	0.6005	41.68	$4.44 \times 10^{-16}$	strong
$\log P_{\text{jet}}$	$\log M$	BL Lacs	0.0314	46.07	0.88	week
$\log P_{\text{jet}}$	$\log B$	FSRQs	-0.6217	49.77	$3.83 \times 10^{-6}$	strong
$\log P_{\text{jet}}$	$\log B$	BL Lacs	0.5949	43.47	$2 \times 10^{-2}$	strong
$\log P_{\text{jet}}$	$\log \eta_m$	FSRQs	0.4512	48.23	$2.64 \times 10^{-6}$	strong
$\log P_{\text{jet}}$	$\log \eta_m$	BL Lacs	0.8101	49	$1.55 \times 10^{-8}$	strong

**Note.** The analysis results, the first column is the dependent variable; the second column is the independent variable; the third column is the class of Fermi blazars; the fourth column is the slope; the fifth column is the intercept; the sixth column is the confidence coefficient; the seventh column is the correlation strength.

In addition, from what is discussed in Daly (2019), the magnetic field can be written as

$$\left(\frac{B}{10^4 G}\right) = \left(\frac{B}{B_{\text{Edd}}}\right) \left(\frac{\kappa_B^2}{M_8}\right)^{1/2} = \left(\frac{L_{\text{bol}}}{g_{\text{bol}} L_{\text{Edd}}}\right)^{A/2} \left(\frac{\kappa_B^2}{M_8}\right)^{1/2}, \quad (24)$$

where  $M_8$  is the black hole mass in units of  $10^8 M_{\odot}$ , the Eddington magnetic field strength in units of  $10^4 G$ ,  $B_{\text{Edd}} \equiv \kappa_B M_8^{-1/2}$ ,  $\kappa_B = 6$  and  $g_{\text{bol}} = 1$ . We apply  $A = 0.43$  and the Eddington luminosity,  $L_{\text{Edd}} = 1.26 \times 10^{38} (M_{\text{BH}}/M_{\odot})$ , in this paper (Begelman et al. 1984; Ho 2009; Daly 2019; Chen et al. 2021).

### 2.7. Jet Power and Beam Power

Cavagnolo et al. (2010) reported that the relationship between average jet power and jet spectral flux at radio

$$P_{\text{jet}} = 5.8 \times 10^{43} \left(\frac{P_{\text{radio}}}{10^{40} \text{ erg s}^{-1}}\right)^{0.64} \text{ erg s}^{-1}. \quad (25)$$

We get the radio luminosity by integrating the radio flux over the 10–5000 MHz frequency band (Machacek et al. 2006).

For the beam power, Willott et al. (1999) and Chen et al. (2021) reported the relationship between beam power and radio luminosity

$$L_j \approx 1.7 \times 10^{45} f^{3/2} \left(\frac{L_{151}}{10^{44} \text{ erg s}^{-1}}\right)^{6/7} \text{ erg s}^{-1}, \quad (26)$$

and where  $1 < f < 20$ , we set  $f = 1$ . This equation is employed to estimate the beam power of blazars. Although this equation is used to estimate the beam power of FR II radio galaxies, many authors also utilize it to estimate the beam power of blazars, because they think FR II radio galaxies have similar radio properties to blazars (Cao 2003; Chen et al. 2015).

## 3. The Results and Discussions

### 3.1. Distribution of Parameters

Figure 2 shows the distributions of redshift. The distributions of FSRQs and BL Lacs are  $0.189 < z < 3.033$  and  $0.051 < z < 2.153$ , respectively. The means of FSRQs and BL Lacs are  $z = 1.283$  and  $z = 0.755$ , respectively. The medians of FSRQs and BL Lacs are  $z = 1.249$  and  $z = 0.717$ , respectively. The Kolmogorov-Smirnov (K-S) test shows that redshifts of FSRQs do not fit a normal distribution ( $p = 0.009$ ), while those of BL

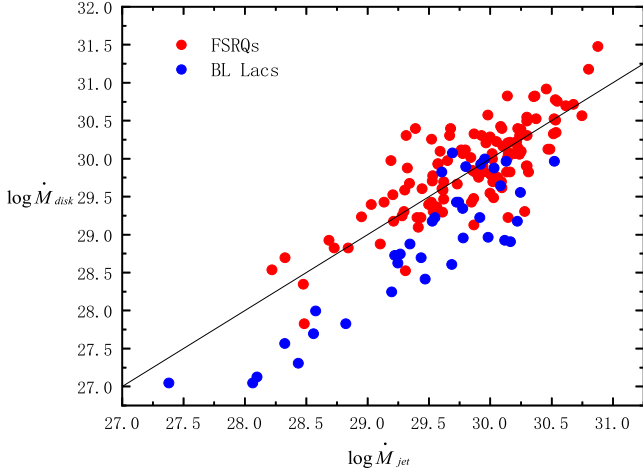


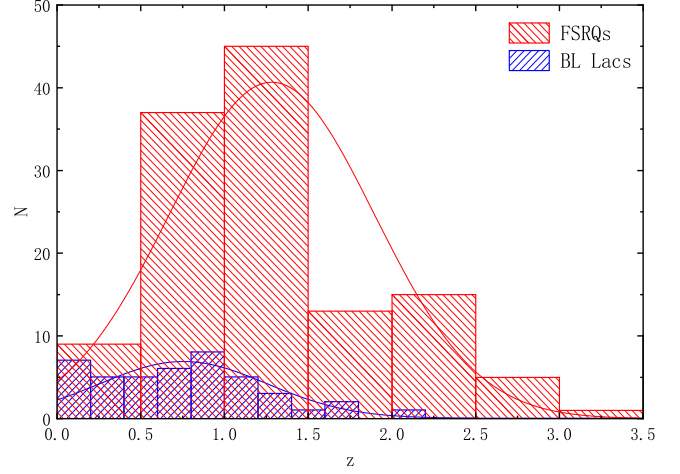
**Figure 1.**  $M_{\text{disk}}^* = L_d/0.1c^2$  vs.  $M_{\text{jet}}^* = P_{\text{jet}}/c^2$  for all samples. The black line stands for the accretion rate calculated by the two methods being the same. FSRQs are near the black line and BL Lac are below the black line.  $M_{\text{jet}}^*$  is greater than  $M_{\text{disk}}^*$  for most BL Lacs, but this aspect has little effect on the correlation analysis.

Lacs do fit a normal distribution ( $p = 0.2$ , we think that when  $p > 0.05$ , it conforms to a normal distribution). The distributions of the redshift of FSRQs and BL Lacs are significantly different. In order to facilitate the observation of the distribution, we fit the data with a normal distribution, as depicted in the plots below.

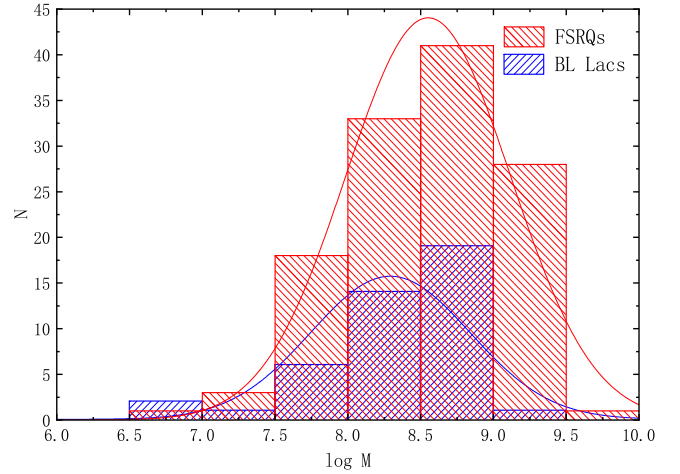
Figure 3 displays the distributions of black hole mass, and the distributions of FSRQs and BL Lacs are  $6.73 < \log M < 9.8$  and  $6.51 < \log M < 9$ , respectively. The means of FSRQs and BL Lacs are  $\log M = 8.55$  and  $\log M = 8.29$ , respectively, and the medians of FSRQs and BL Lacs are  $\log M = 8.62$  and  $\log M = 8.4$ , respectively. Neither FSRQs nor BL Lacs fit a normal distribution (for FSRQs,  $p = 0.023$ , for BL Lacs  $p = 0.012$ ). The distributions of FSRQs and BL Lacs are not much different. The black hole mass can be obtained by different full widths at half maximum (FWHMs) ( $M_{H\beta}$ ,  $M_{Mg II}$ ,  $M_{IV}$ ), resulting in different black hole masses; we chose one of them, but which one is better requires further study.

Figure 4 shows the distributions of accretion disk magnetic field, and the associated distributions of FSRQs and BL Lacs are  $4.15 < \log B < 5.94$  and  $4.09 < \log B < 5.98$ , respectively. The means of FSRQs and BL Lacs are  $\log B = 4.76$  and  $\log B = 4.81$ , respectively, and the medians of FSRQs and BL Lacs are  $\log B = 4.73$  and  $\log B = 4.78$ , respectively. Neither FSRQs nor BL Lacs fit a normal distribution (for FSRQs,  $p = 0.016$ , for BL Lacs  $p = 0.021$ ), and the distributions of FSRQs and BL Lacs are very similar. Accretion disk magnetic field is computed using Equation (20) derived by Daly (2019) through empirical relationships, because an accurate accretion disk magnetic field is difficult to obtain.

Figure 5 shows the distributions of black hole spin, and the associated distributions of FSRQs and BL Lacs are



**Figure 2.** Distributions of redshift; the red and blue lines are the normal distribution curves of FSRQs and BL Lacs, respectively.



**Figure 3.** Distributions of black hole mass (in units of solar mass); the meanings of lines are the same as in Figure 2.

$-1.32 < \log j < -0.04$  and  $-1.48 < \log j < -0.13$ , respectively. The means of FSRQs and BL Lacs are  $\log j = -0.7$  and  $\log j = -0.78$ , respectively, and the medians of FSRQs and BL Lacs are  $\log j = -0.69$  and  $\log j = -0.75$ , respectively. Both FSRQs and BL Lacs are normally distributed (for FSRQs and BL Lacs  $p = 0.2$ ), FSRQs and BL Lacs have exactly the same distribution, and  $j$  is computed by Equation (18).

### 3.2. Black Hole Mass versus Magnetic Field and Black Hole Spin

Equation (21) indicates that

$$\log M = -2 \log B + \log a, \quad (27)$$

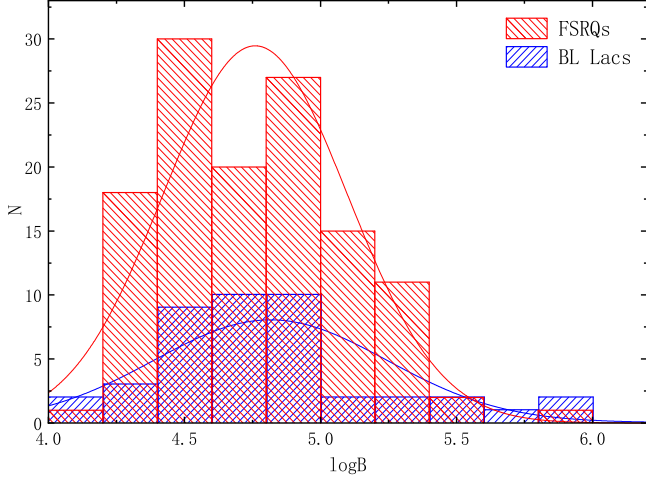


**Figure 4.** Distributions of accretion disk magnetic field; the meanings of lines are the same as in Figure 2.

where  $a = 10^4 \kappa_B \left( \frac{L_{\text{bol}}}{g_{\text{bol}} L_{\text{Edd}}} \right)^{A/2} > 0$ . Figure 6 shows black hole mass as a function of accretion disk magnetic field, for FSRQs

$$\log M = -1.57 \log B + 16.03, \quad (p = 5.21 \times 10^{-59}), \quad (28)$$

and for BL Lacs

$$\log M = -1.16 \log B + 13.89, \quad (p = 2.48 \times 10^{-17}). \quad (29)$$

The linear fits of FSRQs and BL Lacs are similar, but the black hole mass of FSRQs is greater than that of BL Lacs when the magnetic field strength is small. From the linear fits, when FSRQs and BL Lacs have the same black hole mass  $\log M = 7.83$ , they have the same magnetic field strength  $\log B = 5.22$ ; when black hole mass  $\log M > 7.83$  with the same  $M$ , FSRQs have larger magnetic field strength than BL Lacs; when black hole mass  $\log M < 7.83$  with the same  $M$ , BL Lacs have larger magnetic field strength than FSRQs.

Figure 7 shows black hole spin as a function of black hole mass, for FSRQs

$$\log j = -0.075 \log M - 0.062, \quad (p = 0.03), \quad (30)$$

and for BL Lacs

$$\log j = -0.24 \log M - 1.22, \quad (p = 0.04). \quad (31)$$

Both FSRQs and BL Lacs are negatively correlated, that is, when the black hole mass is larger, the black hole spin is slower, and this situation is described in King et al. (2008) and Chen et al. (2021). Possible reasons for the result are isotropic chaotic accretion of black holes or the merging of smaller black holes (Volonteri et al. 2005; Nelson et al. 2014; Fiacconi et al. 2018).

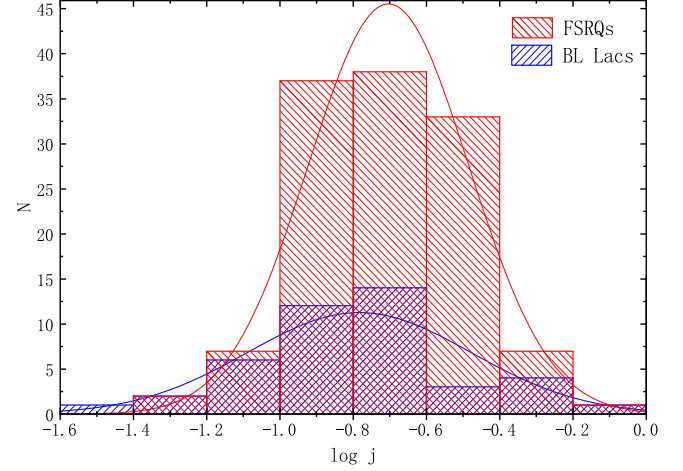


**Figure 5.** Distributions of accretion disk magnetic field; the meanings of lines are the same as in Figure 2.

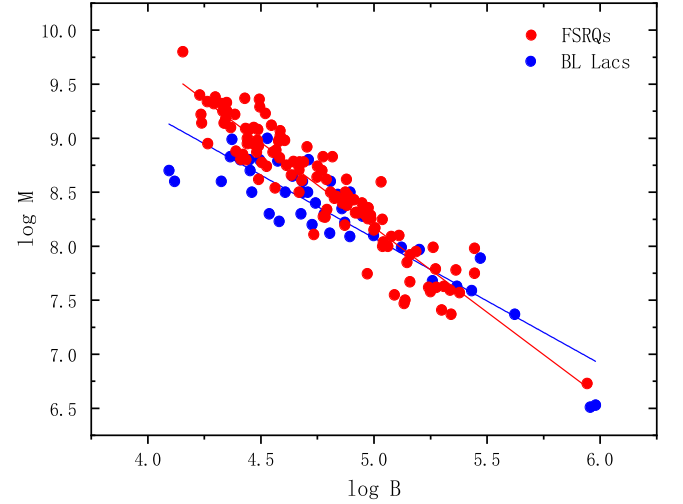


**Figure 6.** The red line is the linear fit of FSRQs, and the blue line is the linear fit of BL Lacs.

### 3.3. Accretion Rate versus Black Hole Spin

Figure 8 plots black hole mass as a function of accretion disk magnetic field, for FSRQs

$$\log \dot{M}_{\text{jet}} = 0.995 \log j + 30.56, \quad (p = 1.55 \times 10^{-6}), \quad (32)$$

and for BL Lacs

$$\log \dot{M}_{\text{jet}} = 1.77 \log j + 30.76, \quad (p = 6.4 \times 10^{-9}). \quad (33)$$

Both FSRQs and BL Lacs are positively correlated, and when accretion disk luminosity and black hole spin are considered, there is a similar relationship. Chen et al. (2021) reported that the third-order fitting is better between  $\log P_{\text{jet}}$  and  $j$ , and the

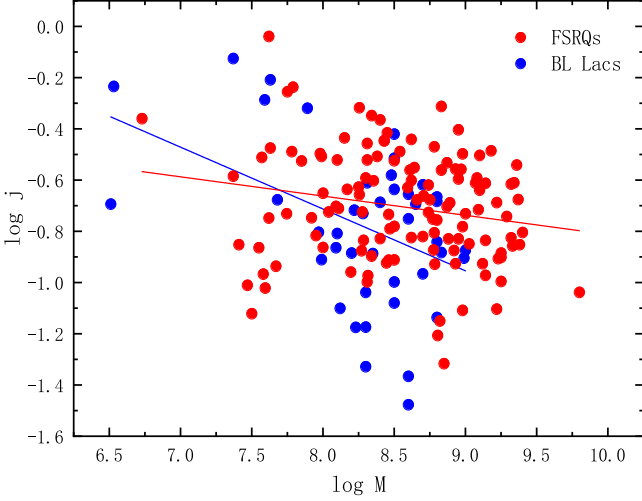


**Figure 7.** The red line is the linear fit of FSRQs, and the blue line is the linear fit of BL Lacs.

numerical simulations in Nemmen et al. (2007) have a similar result. These relationships all indicate that the black hole spin has a promoting effect on the black hole accretion rate.

### 3.4. Intrinsic $\gamma$ -Ray Luminosity

We get the radio luminosity by integrating the radio flux over the 10–5000 MHz frequency band, and  $\gamma$ -ray luminosity by integrating the  $\gamma$ -ray flux over 0.1–100 GHz (Nemmen et al. 2007).  $\gamma$ -rays are produced upstream by IC scattering, however radio is produced by synchrotron emission from the extended jet (Ghisellini & Tavecchio 2009, 2010).  $\gamma$ -ray luminosity is a good indicator of jet power. In order to avoid the beaming effect we use intrinsic  $\gamma$ -ray luminosity,  $L_\gamma^{\text{int}}$ . Figure 9 shows intrinsic  $\gamma$ -ray luminosity as a function of accretion disk luminosity for FSRQs

$$\log L_\gamma^{\text{int}} = 0.6436 \times \log L_{\text{disk}} + 15.32, \quad (p = 2.55 \times 10^{-12}), \quad (34)$$

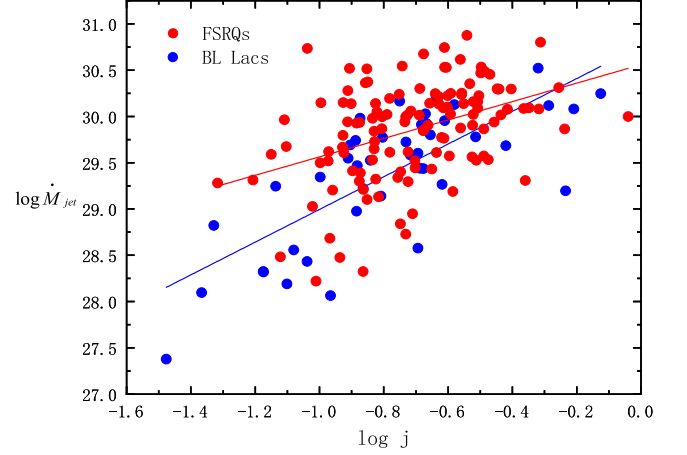
and for BL Lacs

$$\log L_\gamma^{\text{int}} = 0.7098 \times \log L_{\text{disk}} + 12.58, \quad (p = 8.61 \times 10^{-12}). \quad (35)$$

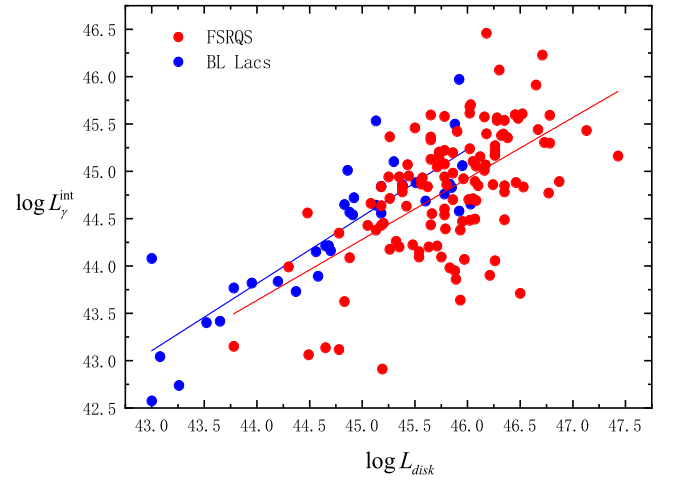
For all sources, the significant relationships between intrinsic  $\gamma$ -ray luminosity and accretion disk luminosity indicate that accretion rate is related to the jet.

Figure 10 depicts intrinsic  $\gamma$ -ray luminosity as a function of black hole mass, for FSRQs

$$\log L_\gamma^{\text{int}} = 0.5582 \times \log M + 40.05, \quad (p = 1.36 \times 10^{-8}), \quad (36)$$



**Figure 8.** The red line is the linear fit of FSRQs, and the blue line is the linear fit of BL Lacs.



**Figure 9.** The red line is the linear fit of FSRQs, and the blue line is the linear fit of BL Lacs.

and for BL Lacs

$$\log L_\gamma^{\text{int}} = 0.0745 \times \log M + 43.7, \quad (p = 0.73). \quad (37)$$

Figure 11 shows intrinsic  $\gamma$ -ray luminosity as a function of black hole spin, for FSRQs

$$\log L_\gamma^{\text{int}} = 0.3829 \times \log j + 45.09, \quad (p = 0.16), \quad (38)$$

and for BL Lacs

$$\log L_\gamma^{\text{int}} = 1.475 \times \log j + 45.47, \quad (p = 2.65 \times 10^{-5}). \quad (39)$$

The intrinsic  $\gamma$ -ray luminosity of FSRQs has a significant positive correlation with the black hole mass, but has no significant correlation with the black hole spin, while the intrinsic  $\gamma$ -ray luminosity of BL Lacs has a significant positive correlation with the black hole spin, but has no significant

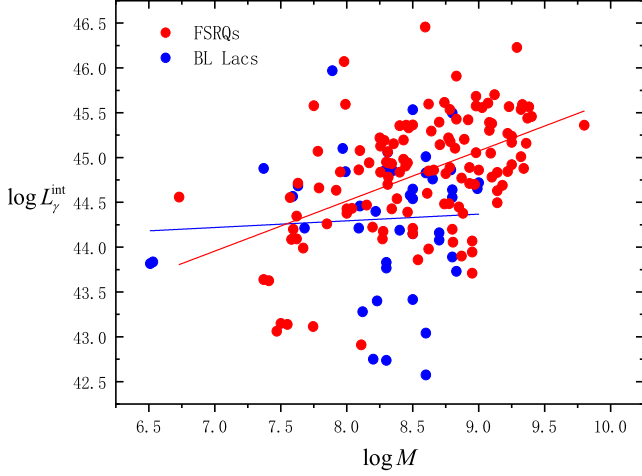


**Figure 10.** The red line is the linear fit of FSRQs, and the blue line is the linear fit of BL Lacs.

correlation with black hole mass. These relationships indicate that the jet power is related to the mass, spin and accretion rate of the black hole, but there are differences between FSRQs and BL Lacs.

### 3.5. Jet Power

In the BP model (Blandford & Payne 1982), the magnetic field lines leave the accretion disk and extend far away, and the angle between the polar component of the magnetic field and the surface of the disk is less than 60 deg; in a hot magnetically dominated corona where the flow is driven by gas pressure, a centrifugally driven outflow of matter from the disk is possible. In the BZ model (Blandford & Znajek 1977), when the magnetic field lines supported by the external current flowing in the equatorial disk pass through the rotating black hole, an electric potential difference is induced. If the field strength is large enough, the vacuum is unstable, and the cascade of electron-positron pairs will create a surrounding force-free magnetic layer. In these cases, that energy and angular momentum will be extracted electromagnetically. Further results show that the charge will never make a significant contribution to the geometry of the rotating black hole.

Figure 12 shows the relationship between jet power and black hole spin, for FSRQs

$$\log P_{\text{jet}} = 0.9954 \times \log j + 47.51, \quad (p = 1.55 \times 10^{-6}), \quad (40)$$

and for BL Lacs

$$\log P_{\text{jet}} = 1.7666 \times \log j + 47.72, \quad (p = 6.4 \times 10^{-9}). \quad (41)$$

From the significant correlation between the jet power and the black hole spin, we think that the BZ model may dominate over the BP model for the samples selected in this paper, indicating that the jet generation extracts the energy of the black hole spin.

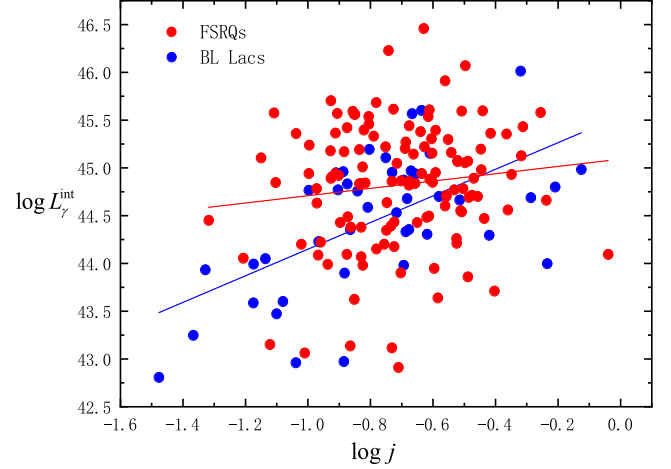


**Figure 11.** The red line is the linear fit of FSRQs, and the blue line is the linear fit of BL Lacs.

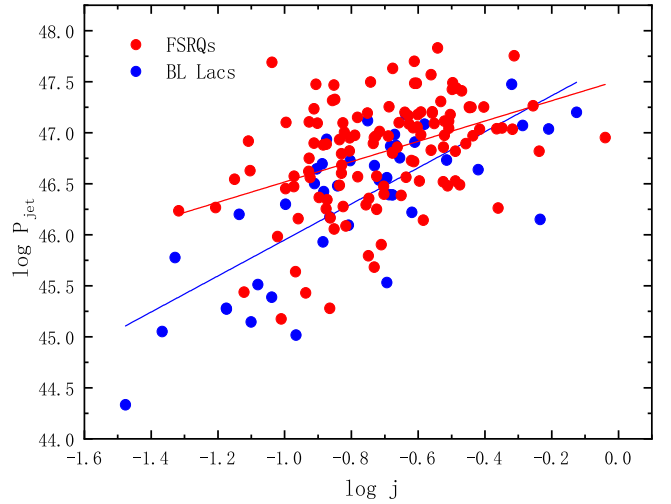


**Figure 12.** The red line is the linear fit of FSRQs, and the blue line is the linear fit of BL Lacs.

In addition, jet power is greater than the accretion disk luminosity for all samples, also tending to favor the BZ model.

Figure 13 displays the relationship between jet power and black hole mass, for FSRQs

$$\log P_{\text{jet}} = 0.6005 \times \log M + 41.68, \quad (p = 4.44 \times 10^{-16}), \quad (42)$$

and for BL Lacs

$$\log P_{\text{jet}} = 0.0314 \times \log M + 46.07, \quad (p = 0.88). \quad (43)$$

The jet power and black hole mass of FSRQs have a significant positive correlation, but not the BL Lacs, which is consistent with the relationship of intrinsic  $\gamma$ -ray luminosity.

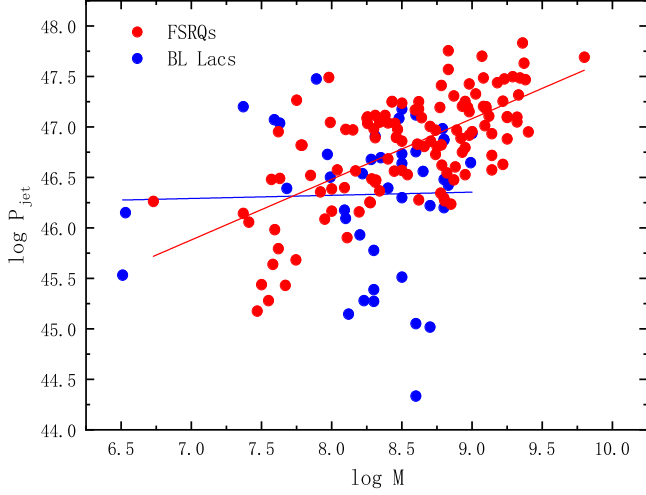


**Figure 13.** The red line is the linear fit of FSRQs, and the blue line is the linear fit of BL Lacs.

Figure 14 shows the relationship between jet power and magnetic field strength, for FSRQs

$$\log P_{\text{jet}} = -0.6217 \times \log B + 49.77, \quad (p = 3.83 \times 10^{-6}), \quad (44)$$

and for BL Lacs

$$\log P_{\text{jet}} = 0.5949 \times \log B + 43.47, \quad (p = 0.02). \quad (45)$$

This figure shows that the jet power and accretion disk magnetic field of FSRQs have a significant negative correlation, while the jet power and accretion disk magnetic field of BL Lacs have a significant positive correlation. For this case, we should consider using the accretion rate  $\log P_{\text{jet}}/c^2$  instead of jet power  $\log P_{\text{jet}}$ .  $\log B$  and  $\log P_{\text{jet}}/c^2$  of FSRQs are negatively correlated, with the form  $\log B = -0.26 \times \log P_{\text{jet}}/c^2 + 12.44$  ( $p = 3.83 \times 10^{-6}$ ), and  $\log B$  and  $\log P_{\text{jet}}/c^2$  of BL Lacs are positively correlated, with the form,  $\log B = 0.21 \times \log P_{\text{jet}}/c^2 - 1.41$  ( $p = 0.02$ ). Without considering the influence of other parameters, FSRQs form an accretion disk during the accretion process, and a magnetic field is generated on the accretion disk. When the magnetic field on the accretion disk becomes an ordered magnetic field, it will affect the accretion of the black hole, suppress the accretion rate and exhibit a negative feedback relationship, while the ordered magnetic field on the accretion disk of BL Lacs will promote the accretion of the black hole and show a positive feedback relationship. The reason for this is unknown and will be further studied in the future.

In the BZ model, the accretion disk magnetic field plays an important role in the generation of jets, which is considered in the multiple linear regression; the multiple linear regression of

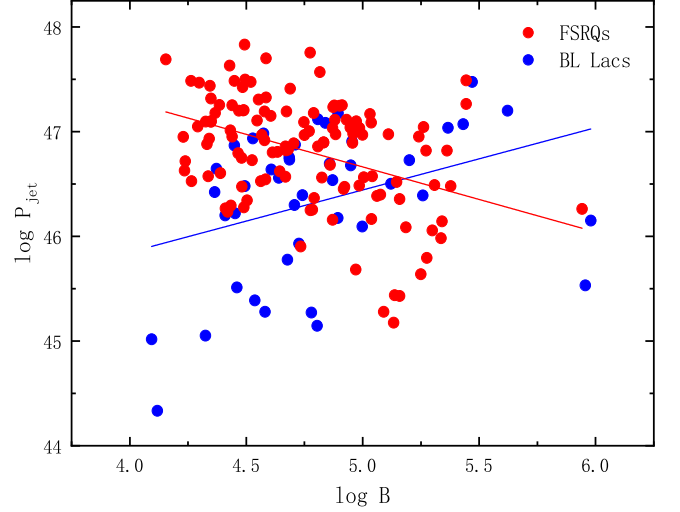


**Figure 14.** The red line is the linear fit of FSRQs, and the blue line is the linear fit of BL Lacs.

the jet power of FSRQs is

$$\log P_{\text{jet}} = 1.685 \times \log M + 0.105 \times \log \dot{M}_{\text{disk}} + 0.874 \times \log j + 1.969 \times \log B + 20.5, \quad (46)$$

with  $p \approx 0$ , and the standardized coefficients of black hole mass, accretion disk luminosity, black hole spin and magnetic field strength are 1.797, 0.118, 0.364 and 1.264, respectively. The contribution rates of each parameter are:

$$\varepsilon_{\log M} = 1.797 / (1.797 + 0.118 + 0.364 + 1.264) \times 100\% = 50.72\%, \quad (47)$$

$$\varepsilon_{\log \dot{M}_{\text{disk}}} = 0.118 / (1.797 + 0.118 + 0.364 + 1.264) \times 100\% = 3.33\%, \quad (48)$$

$$\varepsilon_{\log j} = 0.364 / (1.797 + 0.118 + 0.364 + 1.264) \times 100\% = 10.27\%, \quad (49)$$

$$\varepsilon_{\log B} = 1.264 / (1.797 + 0.118 + 0.364 + 1.264) \times 100\% = 35.68\%. \quad (50)$$

For BL Lacs

$$\log P_{\text{jet}} = 2.079 \times \log M + 0.036 \times \log \dot{M}_{\text{disk}} + 0.858 \times \log j + 2.606 \times \log B + 16.22. \quad (51)$$

With  $p \approx 0$ , the standardized coefficients of black hole mass, accretion disk luminosity, black hole spin and magnetic field strength are 1.702, 0.045, 0.378 and 1.669, respectively. The contribution rates of each parameter are:

$$\varepsilon_{\log M} = 1.702 / (1.702 + 0.045 + 0.378 + 1.669) \times 100\% = 44.86\%, \quad (52)$$

$$\begin{aligned} \varepsilon_{\log \dot{M}_{\text{disk}}} &= 0.045 / (1.702 + 0.045 + 0.378 + 1.669) \times 100\% \\ &= 1.19\%, \end{aligned} \quad (53)$$

$$\begin{aligned} \varepsilon_{\log j} &= 0.378 / (1.702 + 0.045 + 0.378 + 1.669) \\ &\times 100\% = 9.96\%, \end{aligned} \quad (54)$$

$$\begin{aligned} \varepsilon_{\log B} &= 1.669 / (1.702 + 0.045 + 0.378 + 1.669) \\ &\times 100\% = 43.99\%. \end{aligned} \quad (55)$$

From the point of view of contribution rate, there is no significant difference between FSRQs and BL Lacs. The contribution rate of the accretion rate of FSRQs and BL Lacs to the jet power is almost zero, while the contribution rates of the accretion disk magnetic field to the jet power of FSRQs and BL Lacs are as high as 35.68% and 43.99%, respectively. The relationships between  $\log B$  and  $\log \dot{M}_{\text{jet}}$  above affirm that the accretion rate and the accretion disk magnetic field have a significant correlation. It can be considered that the accretion disk magnetic field is the product of the accretion process. It is the accretion disk magnetic field that directly affects the jet during the generation of the jet, but the accretion rate indirectly affects the jet, so the contribution rate of the accretion disk magnetic field can be regarded as the contribution rate of the accretion rate. The black hole masses of FSRQs and BL Lacs have a great contribution rate to the jet, which are 50.72% and 44.86%, respectively, and the contribution rates of the black hole spin of FSRQs and BL Lacs are 10.27% and 9.96%, respectively. The spacetime outside the horizon of an SMBH will be curved, and a rotating black hole has a drag effect on the spacetime outside the horizon; the jet will extract the rotational kinetic energy of the black hole. Obviously, the mass of the black hole has a greater contribution rate.

### 3.6. Generation Efficiency of Jet

The effect of general relativity is obvious where the inside of the accretion disk is close to the black hole. We assumed that all samples can produce a jet and extract the black hole rotation energy, which is not necessarily accurate. Assuming the accretion disk can be modeled as fluids, in the BZ model, for the production of the jet, strong and dynamic magnetic fields are necessary. Since accretion is a long process, it is important to perform multidimensional general relativistic magnetohydrodynamics (GRMHD) simulations. Nakamura et al. (2018) performed extensive inspections of the M87 jet by using two-dimensional (2D) GRMHD simulations and the steady axisymmetric force-free electrodynamic (FFE) solution. The result suggests that the M87 jet is likely powered by a rotating black hole. Mościbrodzka et al. (2016) performed three-dimensional (3D) GRMHD simulations of M87, and the result suggests that the edge-brightening is related to black hole spin. Avara et al. (2016) performed fully 3D GRMHD simulations of thin accretion disks with high radiation efficiency. In the long-

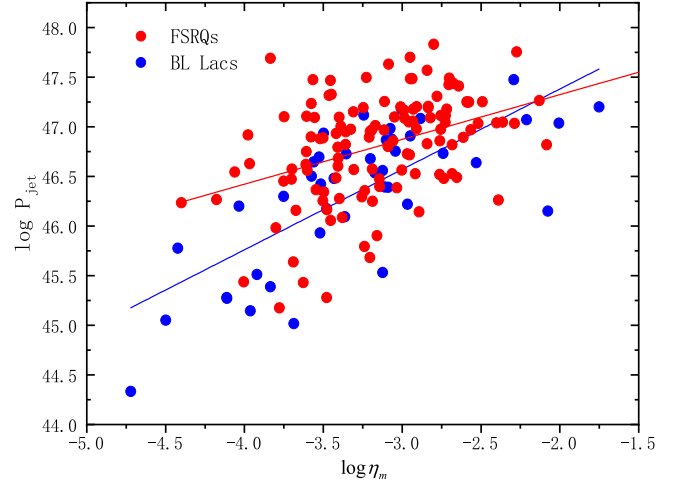


**Figure 15.** The red line is the linear fit of FSRQs, and the blue line is the linear fit of BL Lacs.

term ( $t \sim 70000 r_g/c$ ) evolution simulation, the quasi-steady-state MAD radius is extended to  $t \sim 35 r_g$ , and the radiation efficiency of the accretion disk is 15%. Combining more than 25 different thicker MAD models, Avara et al. found the jet production efficiency in the thin MAD model,

$$\eta_m \approx 4\omega_H^2 \left( 1 + \frac{0.3\omega_H}{1 + 2h^4} \right)^2 h^2, \quad (56)$$

where  $\omega_H \equiv j/r_H$ ,  $r_H = 1 + \sqrt{1 - j^2}$  is the horizon radius and  $h = H/R$  is the disk thickness. In the MAD model, we apply  $h = 0.13$  (Avara et al. 2016) to estimate the jet production efficiency. Figure 15 shows jet power as a function of generation efficiency for a jet; for FSRQs

$$\log P_{\text{jet}} = 0.4512 \log \eta_m + 48.23, \quad (p = 2.64 \times 10^{-6}), \quad (57)$$

and for BL Lacs

$$\log P_{\text{jet}} = 0.8101 \log \eta_m + 49, \quad (p = 1.55 \times 10^{-8}). \quad (58)$$

Both FSRQs and BL Lacs have significant positive correlations between jet power and jet production efficiency. That is, our samples conform to the numerical simulation performed by Avara et al. (2016). The contribution rate of other parameters will be very small after considering black hole spin. Because the jet generation efficiency is computed by black hole spin, we do not consider the black hole spin in the multiple linear regression of the jet production efficiency. The multiple linear regression of the jet generation efficiency of FSRQs is as follows:

$$\begin{aligned} \log \eta_m &= -0.218 \times \log M + 0.508 \times \log \dot{M}_{\text{disk}} \\ &+ 0.583 \times \log B - 27.307, \end{aligned} \quad (59)$$

with  $p = 4.05 \times 10^{-11}$ . The standardized coefficients of black hole mass, accretion disk luminosity and magnetic field

strength are  $-0.258$ ,  $0.633$  and  $0.415$ , respectively. The contribution rates of each parameter are:

$$\begin{aligned} \epsilon_{\log M} &= 0.258 / (0.258 + 0.633 + 0.415) \times 100\% = 19.7\%, \quad (60) \end{aligned}$$

$$\begin{aligned} \epsilon_{\log \dot{M}_{\text{disk}}} &= 0.633 / (0.258 + 0.633 + 0.415) \times 100\% = 48.5\%, \quad (61) \end{aligned}$$

$$\begin{aligned} \epsilon_{\log B} &= 0.415 / (0.258 + 0.633 + 0.415) \times 100\% = 31.8\%. \quad (62) \end{aligned}$$

For BL Lacs

$$\begin{aligned} \log \eta_m &= -0.271 \times \log M + 0.387 \times \log \dot{M}_{\text{disk}} \\ &+ 0.472 \times \log B - 20.613, \quad (63) \end{aligned}$$

with  $p = 4.12 \times 10^{-9}$ . The standardized coefficients of black hole mass, accretion disk luminosity and magnetic field strength are  $-0.234$ ,  $0.514$  and  $0.319$ , respectively. The contribution rates of each parameter are:

$$\begin{aligned} \epsilon_{\log M} &= 0.234 / (0.234 + 0.514 + 0.319) \times 100\% = 21.9\%, \quad (64) \end{aligned}$$

$$\begin{aligned} \epsilon_{\log \dot{M}_{\text{disk}}} &= 0.514 / (0.234 + 0.514 + 0.319) \times 100\% = 48.2\%, \quad (65) \end{aligned}$$

$$\begin{aligned} \epsilon_{\log B} &= 0.319 / (0.234 + 0.514 + 0.319) \times 100\% = 29.9\%. \quad (66) \end{aligned}$$

The contribution rate of the black hole mass to the jet generation efficiency is negative, about 20%. That is, without considering other parameters, the larger the black hole mass is, the lower the jet generation efficiency, while the contribution rates of the accretion rate and the accretion disk magnetic field are positive, and the combined contribution rate is about 80%. This result is taken for granted. The relationship between black hole spin and black hole mass above shows that a black hole with higher spin has smaller mass. Under the premise that the black hole spin has a significant contribution to the jet generation, the smaller the black hole mass is, the higher the jet generation efficiency. The relationship between black hole spin and accretion rate in the previous section shows that the black hole spin has a promoting effect on the accretion rate, but as the black hole (long-term isotropic chaotic) accretion process proceeds, the black hole spin will slow down. For this, it is necessary to examine the contribution rate of the black hole mass and spin to the accretion rate. We used a multiple linear regression between  $\log L_{\text{disk}}$ ,  $\log M$  and  $\log j$  to calculate the contribution rate. The contributions of the black hole mass and black hole spin of FSRQs to the accretion rate are 69.2% and 30.8%, respectively, and the contributions of the black hole mass and black hole spin of BL Lacs to the accretion rate are 36.4% and 63.6%, respectively. Combining what is discussed

above, a possible explanation is that BL Lacs and FSRQs are objects from the same class, but BL Lacs occur in the early stage of FSRQs. At this time, the BL Lacs have relatively smaller mass with relatively higher spin. Also, the spacetime drag effect caused by the black hole spin causes strong magnetic reconnection at the inner radius of the accretion disk to generate a strong magnetic field, so that BL Lacs can generate powerful jets. The accretion of material at this time is dominated by the black hole spin, and as the accretion process proceeds, the mass increases and the spin becomes slower. Then, the accretion model may change. BL Lacs gradually become FSRQs. At this time, the spacetime drag effect caused by the spin of the black hole is relatively weak, but there is still a strong magnetic field to generate jets, and the accretion of material at this time is dominated by the black hole mass.

#### 4. Summary and Conclusions

In Figure 6, the data points are basically concentrated in the area  $\log B < 5.22$ , where the black hole mass of FSRQs is generally greater than that of BL Lacs. From this, it can be considered that BL Lacs may occur earlier than FSRQs. With the evolution of the accretion process, the accretion disk magnetic field becomes stronger. When the magnetic field reaches a critical value, the magnetic field of the accretion disk gradually weakens. This evolutionary process results in FSRQs and BL Lacs that may have the same accretion disk magnetic field but FSRQs have a larger black hole mass, where the area  $\log B > 5.22$  can be considered as the intermediate state of BL Lacs to FSRQs.

For FSRQs or BL Lacs, as the black hole mass increases, the black hole spin becomes slower, i.e.,  $\log j \propto -\log M$ . The possible reason is long-term isotropic chaotic accretion. The angular momentum of the black hole is conserved. As the isotropic chaotic accretion proceeds, the mass of the black hole increases and the spin slows down. It may also be the result of merging with a small-mass black hole, which is similar to reverse accretion. The angular momentum of a small-mass black hole is opposite to the direction of the black hole spin, which causes the black hole spin to slow. When the black hole spin becomes slower, the spacetime drag effect caused by the black hole spin becomes weaker, and the accretion disk magnetic field weakens, i.e.,  $\log j \propto \log B$ . At the same time, the mass of the black hole increases, i.e.,  $\log B \propto -\log M$ .

Xiong & Zhang (2014) found the dividing line  $L_{\text{BLR}}/L_{\text{Edd}} \sim 5 \times 10^{-4}$  between FSRQs and BL Lacs from the relationship between  $\log L_{\text{BLR}}/L_{\text{Edd}}$  and  $\log L_{\gamma}/L_{\text{Edd}}$ . Sbarato et al. (2012) obtained the same result, and the similar dividing line in this paper is  $L_{\text{BLR}}/L_{\text{Edd}} \sim 5 \times 10^{-2}$ , which is different from the results of Xiong and Sbarato. Ghisellini (2010) obtained the dividing line  $L_{\text{disk}}/L_{\text{Edd}} \sim 10^{-2}$  between FSRQs and BL Lacs from the relationship between  $\log L_{\text{disk}}/L_{\text{Edd}}$  and  $\log \dot{M}/\dot{M}_{\text{Edd}}$ . Our samples have almost

exactly the same dividing line. The magnitude of the accretion rate affects the magnitude of  $L_{\text{disk}}$  and  $L_{\text{BLR}}$ , so it can be considered that Xiong and Zhang, Sbarrato et al. and Ghisellini indirectly used the accretion rate to classify blazars. In the process of black hole accretion evolution, the accretion disk will generate an ordered magnetic field and affect the accretion rate and jet power. Therefore, the contribution of the accretion disk magnetic field to the accretion rate and jet flow is considered. From the multiple linear regression, we find that there is no significant difference in dimensionless accretion rate between FSRQs and BL Lacs, and the magnetic field contributes the most. The generation of jets is also affected by the accretion disk magnetic field. From the linear fitting of  $\log P_{\text{jet}}$  and  $\log B$  in Figure 14, it can be seen that the jet power of FSRQs is inhibited by the magnetic field of the accretion disk, while for BL Lacs the situation is the opposite. The possible reason for this is that the accretion disk magnetic field continues to increase during the evolution of BL Lacs into FSRQs until the accretion disk magnetic field of BL Lacs reaches the critical value. If there are factors that inhibit the accretion disk magnetic field of BL Lacs, the magnetic field strength will not increase to a very high level. Data show that the accretion rate and accretion disk magnetic field of BL Lacs are mutually reinforcing, so that the accretion disk magnetic field can increase to a high value. When the magnetic field reaches the critical value, and the accretion rate also reaches the maximum, the accretion model may change. At this time, the accretion rate and the accretion disk magnetic field inhibit each other, so that the accretion disk magnetic field gradually becomes weaker, which may be the reason for Figure 6. Here we analyze the evolution of BL Lacs from the perspective of increasing black hole mass. BL Lacs with smaller mass evolve into FSRQs. We notice that the mean mass of BL Lacs is smaller than that of FSRQs, but the black hole spin of BL Lacs is slower than that of FSRQs. If analyzed from the perspective of black hole spin, it is not impossible that FSRQs with higher spin evolve into BL Lacs. If both of these scenarios are possible, the continuous evolution of blazars would be possible.

The intrinsic  $\gamma$ -ray luminosity of FSRQs has a significant positive correlation with the accretion disk luminosity and black hole mass, but no significant correlation with the black hole spin, while the intrinsic  $\gamma$ -ray luminosity of BL Lacs has a significant positive correlation with the accretion disk luminosity and black hole spin, but no correlation with black hole mass. This situation is not necessarily consistent with the evolution, because the jet power of FSRQs has a significant correlation with the black hole spin. A possible reason is that a considerable part of the  $\gamma$ -ray photons of FSRQs is produced by the EC mechanism.

Figure 12 shows that the samples are completely consistent with the BZ model. The jet generation efficiency and jet power of FSRQs and BL Lacs are almost the same, indicating that the

jet generation mechanism of FSRQs and BL Lacs may be the same. Jet power is greatly affected by the black hole mass (the contribution rate is over 44%), and is very little affected by the accretion rate (the contribution rate is about 3%), while the jet generation efficiency is relatively weakly affected by the black hole mass (the contribution rate is about 20%), and is relatively greatly affected by the accretion rate (the contribution rate is about 50%). Black hole spin energy is governed by black hole mass and rotational speed. In the BZ model, jet power is directly related to the black hole spin and mass. Part of the contribution rate of the accretion rate is transferred to the contribution rate of magnetic field. The jet power is indirectly related to the accretion rate, resulting in a very low contribution rate. While the generation efficiency of jets is also related to the black hole mass, part of the contribution rate of black hole mass is transferred to the contribution rate of accretion rate. This results in a lower contribution rate of the black hole mass and a higher contribution rate of the accretion rate. The contribution rate of the magnetic field to the jet power is about 40% (for FSRQs, 35.68%, for BL Lacs, 43.99%). The contribution rate of the magnetic field to the jet generation efficiency is about 30%. The jet power is slightly more affected by the magnetic field, but the difference is not obvious. The difference is that the effect of the magnetic field on the jet power is during the BZ process, while the effect of the magnetic field on the jet generation efficiency is before the BZ process. In the hybrid model, Meier (1999) thinks that the generation of a jet is related to the magnitude of the magnetic field, such that for high enough spin, the black hole triggers the magnetic switch, producing relativistic jets. The samples selected have strong accretion disk magnetic field, high enough spin and can generate powerful jets, which are consistent with Meier's theory.

The basic parameters mentioned in the article have uncertainties, some of them even exceeding 0.5 dex, and we have to admit that these interpretations are just a bold attempt. In addition, our work can give others an idea to understand the relationship between the fundamental parameters of black holes.

## Acknowledgments

This work is supported by the National Natural Science Foundation of China (NSFC, grant No.11063004). We thank the experts for their advice.

## ORCID iDs

H. Zhang  <https://orcid.org/0000-0001-6741-1152>

## References

- Avara, M. J., McKinney, J. C., & Reynolds, C. S. 2016, *MNRAS*, 462, 636  
 Begelman, M. C., Blandford, R. D., & Rees, M. J. 1984, *RvMP*, 56, 255  
 Blandford, R., Meier, D., & Readhead, A. 2019, *ARA&A*, 57, 467

- Blandford, R. D., & Payne, D. G. 1982, *MNRAS*, **199**, 883
- Blandford, R. D., & Znajek, R. L. 1977, *MNRAS*, **179**, 433
- Calderone, G., Ghisellini, G., Colpi, M., et al. 2013, *MNRAS*, **431**, 210
- Cao, X. 2003, *ApJ*, **599**, 147
- Cavagnolo, K. W., McNamara, B. R., Nulsen, P. E. J., et al. 2010, *ApJ*, **720**, 1066
- Celotti, A., & Fabian, A. C. 1993, *MNRAS*, **264**, 228
- Celotti, A., & Ghisellini, G. 2008, *MNRAS*, **385**, 283
- Chen, Y., Gu, Q., Fan, J., et al. 2021, *ApJ*, **913**, 93
- Chen, Y.-Y., Zhang, X., Xiong, D., et al. 2015, *AJ*, **150**, 8
- Daly, R. A. 2019, *ApJ*, **886**, 37
- Daly, R. A., Stout, D. A., & Mysliwiec, J. N. 2018, *ApJ*, **863**, 117
- Donato, D., Ghisellini, G., Tagliaferri, G., et al. 2001, *A&A*, **375**, 739
- Fiacconi, D., Sijacki, D., & Pringle, J. E. 2018, *MNRAS*, **477**, 3807
- Fossati, G., Celotti, A., Ghisellini, G., et al. 1997, *MNRAS*, **289**, 136
- Frank, J., King, A., & Raine, D. J. 2002, in *Accretion Power in Astrophysics*, ed. J. Frank, A. King, & D. Raine (Cambridge, UK: Cambridge Univ. Press), 398
- Ghisellini, G. 2010, in *Accretion and Ejection in AGN: a Global View*, 427 (Como: ASPC), 249
- Ghisellini, G. 2016, *Galax*, **4**, 36
- Ghisellini, G., & Tavecchio, F. 2008, *MNRAS*, **387**, 1669
- Ghisellini, G., & Tavecchio, F. 2009, *MNRAS*, **397**, 985
- Ghisellini, G., & Tavecchio, F. 2010, *MNRAS*, **409**, L79
- Ghisellini, G., Tavecchio, F., Foschini, L., et al. 2010, *MNRAS*, **402**, 497
- Ghisellini, G., Tavecchio, F., Maraschi, L., et al. 2014, *Natur*, **515**, 376
- Giommi, P., Polenta, G., Lähteenmäki, A., et al. 2012, *A&A*, **541**, A160
- Ho, L. C. 2009, *ApJ*, **699**, 626
- Hovatta, T., Valtaoja, E., Tornikoski, M., et al. 2009, *A&A*, **494**, 527
- King, A. R., Pringle, J. E., & Hofmann, J. A. 2008, *MNRAS*, **385**, 1621
- Machacek, M., Nulsen, P. E. J., Jones, C., et al. 2006, *ApJ*, **648**, 947
- Mannheim, K., & Biermann, P. L. 1992, *A&A*, **253**, L21
- Maraschi, L., & Tavecchio, F. 2003, *ApJ*, **593**, 667
- McKinney, J. C., Tchekhovskoy, A., & Blandford, R. D. 2012, *MNRAS*, **423**, 3083
- McLure, R. J., & Dunlop, J. S. 2004, *MNRAS*, **352**, 1390
- Meier, D. L. 1999, *ApJ*, **522**, 753
- Meier, D. L. 2001, *ApJL*, **548**, L9
- Mościbrodzka, M., Falcke, H., & Shiokawa, H. 2016, *A&A*, **586**, A38
- Nakamura, M., Asada, K., Hada, K., et al. 2018, *ApJ*, **868**, 146
- Narayan, R., Garcia, M. R., & McClintock, J. E. 1997, *ApJL*, **478**, L79
- Nelson, K., Lau, E. T., & Nagai, D. 2014, *ApJ*, **792**, 25
- Nemmen, R. S., Bower, R. G., Babul, A., et al. 2007, *MNRAS*, **377**, 1652
- Nemmen, R. S., Georganopoulos, M., Guiriec, S., et al. 2012, *Science*, **338**, 1445
- Netzer, H. 2013, in *The Physics and Evolution of Active Galactic Nuclei*, ed. H. Netzer (Cambridge: Cambridge Univ. Press)
- Peterson, B. M., & Wandel, A. 2000, *ApJL*, **540**, L13
- Rawlings, S., & Saunders, R. 1991, *Natur*, **349**, 138
- Rees, M. J. 1984, *Annual Review of Astronomy and Astrophysics*, **22**, 471
- Reynolds, C. S. 2019, *NatAs*, **3**, 41
- Sbarrato, T., Ghisellini, G., Maraschi, L., et al. 2012, *MNRAS*, **421**, 1764
- Shakura, N. I., & Sunyaev, R. A. 1973, *A&A*, **24**, 337
- Shaw, M. S., Romani, R. W., Cotter, G., et al. 2012, *ApJ*, **748**, 49
- Sikora, M., Begelman, M. C., & Rees, M. J. 1994, *ApJ*, **421**, 153
- Stratta, G., Capalbi, M., Giommi, P., et al. 2011, arXiv:1103.0749
- Tchekhovskoy, A., Narayan, R., & McKinney, J. C. 2010, *ApJ*, **711**, 50
- Urry, C. M., & Padovani, P. 1995, *PASP*, **107**, 803
- Volonteri, M., Madau, P., Quataert, E., et al. 2005, *ApJ*, **620**, 69
- Wang, J.-M., Du, P., Hu, C., et al. 2014, *ApJ*, **793**, 108
- Willott, C. J., Rawlings, S., Blundell, K. M., et al. 1999, *MNRAS*, **309**, 1017
- Xie, G. Z., Dai, H., Mao, L. S., et al. 2006, *AJ*, **131**, 1210
- Xie, G. Z., Zhou, S. B., & Liang, E. W. 2004, *AJ*, **127**, 53
- Xiong, D. R., & Zhang, X. 2014, *MNRAS*, **441**, 3375
- Xue, R., Luo, D., Du, L. M., et al. 2016, *MNRAS*, **463**, 3038
- Yu, X., Zhang, X., Zhang, H., et al. 2015, *Ap&SS*, **357**, 14
- Yuan, F., & Narayan, R. 2014, *ARA&A*, **52**, 529